Experimental Neurology 374 (2024) 114714

Contents lists available at ScienceDirect

Experimental Neurology

journal homepage: www.elsevier.com/locate/yexnr

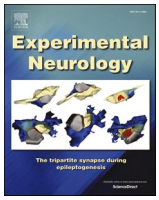

Research paper

The cellular senescence response and neuroinflammation in juvenile mice following controlled cortical impact and repetitive mild traumatic brain injury

Zahra F. Al-Khateeb [a,*], Hasna Boumenar [a], Joycee Adebimpe [a], Shenel Shekerzade [a], Siân M. Henson [b], Jordi L. Tremoleda [a], Adina T. Michael-Titus [a]

[a] Centre for Neuroscience, Surgery and Trauma, The Blizard Institute, Barts and The London School of Medicine and Dentistry, Queen Mary University of London, London, United Kingdom
[b] Translational Medicine and Therapeutics, William Harvey Research Institute, Barts and The London School of Medicine and Dentistry, Queen Mary University of London, London, UK

ARTICLE INFO

Keywords:
Cellular senescence
Neuroinflammation
Traumatic brain injury
Controlled cortical impact
Repetitive mild traumatic brain injury
Juvenile
Mice

ABSTRACT

Traumatic brain injury (TBI) is a leading cause of disability and increases the risk of developing neurodegenerative diseases. The mechanisms linking TBI to neurodegeneration remain to be defined. It has been proposed that the induction of cellular senescence after injury could amplify neuroinflammation and induce long-term tissue changes. The induction of a senescence response post-injury in the immature brain has yet to be characterised. We carried out two types of brain injury in juvenile CD1 mice: invasive TBI using controlled cortical impact (CCI) and repetitive mild TBI (rmTBI) using weight drop injury. The analysis of senescence-related signals showed an increase in γH2AX-53BP1 nuclear foci, p53, p19ARF, and p16INK4a expression in the CCI group, 5 days post-injury (dpi). At 35 days, the difference was no longer statistically significant. Gene expression showed the activation of different senescence pathways in the ipsilateral and contralateral hemispheres in the injured mice. CCI-injured mice showed a neuroinflammatory early phase after injury (increased Iba1 and GFAP expression), which persisted for GFAP. After CCI, there was an increase at 5 days in p16INK4, whereas in rmTBI, a significant increase was seen at 35 dpi. Both injuries caused a decrease in p21 at 35 dpi. In rmTBI, other markers showed no significant change. The PCR array data predicted the activation of pathways connected to senescence after rmTBI. These results indicate the induction of a complex cellular senescence and glial reaction in the immature mouse brain, with clear differences between an invasive brain injury and a repetitive mild injury.

1. Introduction

Traumatic brain injury (TBI) is a leading cause of disability and death in adults as well as children and adolescents (Van Deynse et al., 2019). TBI occurs when an external blow (closed head injury), a penetrative impact (invasive head injury), or a blast wave damages the brain. Even in its milder forms, TBI can cause long-term behavioural and physiological impairments, in addition to increasing the risk of developing neurodegenerative diseases. Most research has focused on the impact of TBI on the mature brain, and it may be assumed that the regenerative capacity of immature brains reduces the impact of injury. However, evidence suggests that patients injured at a young age may be susceptible to long-term behavioural impairments (Cole et al., 2008). TBI in the juvenile brain could have worse outcomes compared to similar injury severity in the adult brain, because of the likely disruptive effect of the injury on neurodevelopmental processes (Dennis et al., 2014). Therefore, there is growing interest in analysing the effect of brain injuries on immature brains. Furthermore, sports-related brain concussions in young children and adolescents are a matter of significant concern (Halstead et al., 2018), because of their potential long-term impact on a

Abbreviations: ROS, Reactive oxygen species; SA-β-gal, senescence-associated β-galactosidase; DDR, DNA damage response; SAHF, senescence-associated heterochromatin foci.

* Corresponding author at: Centre for Neuroscience, Surgery and Trauma, Blizard Institute, Queen Mary University of London, 4 Newark Street, London E1 2AT, United Kingdom.
E-mail address: z.f.h.al-khateeb@qmul.ac.uk (Z.F. Al-Khateeb).

https://doi.org/10.1016/j.expneurol.2024.114714
Received 5 September 2023; Received in revised form 11 December 2023; Accepted 3 February 2024
Available online 5 February 2024

brain which is still in development.

The primary causes of injury in children are falls followed by motor vehicle accidents (Araki et al., 2017; Chen et al., 2018). Falls are associated with concussion-type injuries, while motor vehicle accidents typically result in a mixed type of injury, combining elements of concussion and invasive injury.

The models we have used in the present study were selected because they closely mirror the types of TBI injuries observed clinically in paediatric and young adult populations. For invasive injuries, we selected the controlled cortical impact (CCI) model, a well-established injury model. As for repetitive mild TBI (rmTBI), to model concussions, various injury models and protocols are available in the literature, with significant variability in the number of impacts and the time intervals between each impact. We chose the weight drop injury model (WDI) proposed by Bittigau et al. (1998) for the closed-head injury as it closely models the mechanical forces observed in sports-related injuries, particularly the acceleration-deceleration motion, which results in diffuse brain injury. We selected the specific number of impacts and time intervals based on a preliminary experiment in our group (data not shown in this manuscript) and also guided by existing literature (reviewed by Fehily and Fitzgerald, 2017; Hoogenboom et al., 2019).

Evidence indicates that TBI triggers cellular senescence (Katano et al., 2000; Ritzel et al., 2019; Schober et al., 2010; Schwab et al., 2021; Schwab et al., 2022; Tominaga et al., 2019). Senescence is a stable cell cycle arrest that is triggered by different cellular stressors, such as unrepaired DNA damage, telomere damage/erosion, oncogene activation, reactive oxygen species (ROS), unresolved unfolded protein response and lysosomal stress (Baker and Petersen, 2018; Sharpless and Sherr, 2015). Senescence signals can be detected in neurons and glial cells, and a strong link has been suggested between senescence and neurodegenerative diseases, such as Alzheimer's disease (AD) and Parkinson's disease (PD) (Carreno et al., 2021; Sikora et al., 2021; Spilsbury et al., 2015; Vazquez-Villaseñor et al., 2020).

Mature neurons re-enter the cell cycle under stress linked to excitotoxicity, oxidative stress and the DNA damage response (which all occur in TBI). Elevated expression of markers associated with cell cycle activation in neurons, such as E2F5, c-myc, PCNA, cyclin D1, and CDK4, support evidence of cell cycle re-entry. The increased expression of these markers also primes apoptotic cascades, leading to cell death unless blocked by appropriate survival signals (Folch et al., 2012; Frade and Ovejero-Benito, 2015; Stoica et al., 2009). All of these elements have been identified in the context of TBI (Byrnes and Faden, 2007; Stoica et al., 2009). TBI stimulates cell cycle re-entry which may either lead to apoptosis or proliferation of cells, depending on the cell type (Kabadi et al., 2012). This activation in mature neurons leads to apoptosis (Greene et al., 2004) and it is speculated that neurons would trigger senescence pathways to avoid apoptosis, by increasing the expression of factors including p16INK4a, p53 and p21, thus causing cell cycle arrest. Such senescence markers have been reported after TBI in the adult brain (Katano et al., 2000; Ritzel et al., 2019; Schober et al., 2010; Schwab et al., 2021; Schwab et al., 2022; Tominaga et al., 2019). In the case of senescence reported in TBI in adult mice, Tominaga et al. (2019) showed an increase in β-gal positive cells in the injured hemisphere from day 4 post injury, which peaked at day 7. They also detected the expression of cyclin D1 and proliferative PCNA markers in neurons, astrocytes, and microglia, confirmed by RNA analysis. These results show that the cells, including neurons, re-entered the cell cycle after TBI and that senescence markers levels were elevated following this increase.

However, it is unknown whether brain injury in the juvenile brain can trigger a senescence response - after mild or severe injury. In this study we addressed this question and characterised the effects of traumatic injury on the juvenile brain in the two models of injury: a single invasive injury using the CCI model and rmTBI induced using a closed skull weight drop model. We assessed senescence markers in parallel with markers of neuroinflammation, and changes were assessed at two times post-injury, to detect the dynamics of the response.

2. Materials and methods

2.1. Animals

Juvenile (4–5 weeks old) male CD1 mice, weighing 25–29 g at the start of the study, were used in the experiments (Charles River UK Ltd., Margate, UK). Upon arrival, animals were assigned to cages and remained in the same social group throughout the study. Mice were housed in groups of 3 in standard ventilated cages (Allentown Europe, UK), at 21 ± 1 °C room temperature, 55% ± 10% relative humidity, and a 12-h light: dark cycle, with 06:00–18:00 light and 18:00–06:00 dark. All animals were provided with water and standard chow (Labdiet® EURodent 14% Diet 5LF2, Labdiet, Brentwood, Missouri, U.S.) ad libitum and with environmental enrichment (nesting, tunnel) cages. Animals were acclimatised to the animal unit for a minimum of 7 days. All animal procedures were approved by the Animal Welfare and Ethical Review Body, at Queen Mary University of London and the UK Home Office, conforming to the UK Animals (Scientific Procedures) Act, 1986, and the associated guidelines.

2.2. Controlled cortical impact (CCI)

The CCI model was used to model a moderate invasive TBI. Animals were anaesthetized using a mixture of ketamine (50 mg/kg; Narketan, Vetoquinol, UK) and medetomidine (0.5 mg/kg; (Domitor@OrionPharma, UK) in sterile saline i.p.; 5 ml/kg). A right lateral craniotomy (3.5 mm diameter) was performed under aseptic conditions, and injury was induced using a 3 mm impactor tip, with a speed of 3 m/s, a depth of 2.2 mm and a dwell time of 100 msec, applied using the PCI3000 Precision Cortical Impactor™ (Hatteras Instruments, Inc., Cary, NC), at coordinates 2.0 mm behind bregma and 2.5 mm lateral to the midline. After injury, the skull flap was placed back unfixed to allow for expansion, and the skin was sutured. Analgesia (buprenorphine 0.05 mg/kg, s.c.; Vetergesic, Ceva Animal Health Ltd., UK) was used in all animals preemptively and postoperatively every 12 h (up to 3 days post-surgery). A control group underwent craniotomy (Cranio) only. Naïve animals were not subjected to any intervention.

2.3. Repetitive mild traumatic brain injury (rmTBI)

The weight drop injury (WDI) model was used to replicate a closed skull rmTBI. Animals were briefly exposed to anaesthesia (4% isoflurane in O_2 for 2 min) and placed on tissue paper under a vertical PVC tube and 10 cm above a foam cushion. An 80-g weight was dropped from a height of 40 cm on the head of the mice; the hit was on the scalp midline. As a result of the impact, mice fell through the tissue paper and landed on a foam cushion, thus mimicking an acceleration/deceleration force. This process was carried out 6 times, every 48 h (Fig. A.1, B). The sham group received repeated anaesthesia only (rSham), and the naïve group had no intervention.

2.4. Modified neurological severity score (mNSS)

The modified neurological severity score (mNSS) test was used to evaluate the general motor activity, balance and alertness of the animals, as described (Beni-Adani et al., 2001). The scoring system is based on the ability of mice to perform 10 tasks, which include exiting a 30-cm circle within 2 min, walking straight, having a startle reaction, showing seeking behaviour, absence of mono- or hemiparesis, balance on a 0.5-cm wide beam, balance on a 0.5-cm-diameter round stick, and the ability to walk on 3-, 2-, and 1-cm-wide beams. For the CCI experiment, testing was done every other day until the 9th day post-surgery (Fig. A.1, A, C). For the rmTBI experiment, testing was performed 24 h after each injury session (Fig. A.1, B, D).

2.5. Animal culling and sample collection

For immunostaining, animals were terminally anaesthetised (pentobarbital sodium, Pentoject® 200 mg/mls; Animalcare Limited, UK) and received a cardiac perfusion of phosphate-buffered saline (PBS) and 4% paraformaldehyde (PFA). After decapitation, the brain (including the cerebellum) was extracted and post-fixed in 4% PFA for 24 h, then transferred to 70% ethanol and stored at 4°°C until processing using paraffin embedding. For PCR array, animals were terminally anaesthetised and received a cardiac perfusion of PBS. Brain tissue was snap-frozen and stored at −80 °C.

2.6. Immunostaining

Immunostaining was performed on 8 μm coronal sections cut between bregma −1.9 mm and − 2.1 mm, where the lesion was located. Sections were deparaffinised and hydrated in a series of ethanol (EtOH) baths, then treated with antigen retrieval solution (10 mM citric buffer, pH 6.0, 10 min, microwave). They were blocked with 8% bovine serum albumin (BSA), 0.5% Tween-20 and 0.1% Triton X-100 in PBS overnight at 4 °C. On the next day, sections were washed in 0.5% Tween-20 and 0.1% Triton X-100 in PBS (PBS-TT) and then incubated with primary antibodies (Table 1) overnight at 4 °C. Markers were visualised using secondary goat-raised antibodies, labelled with either Alexa 488 or Alexa 555 (Invitrogen, United States; 1:250), and nuclei were visualised using Hoechst 33342 stain (Tocris Bioscience, United Kingdom; 1:500). Slides were mounted and cover-slipped using Vectashield fluorescent mounting medium (Vector Laboratories, United States).

2.7. Quantification of immunostaining

Four sections were used per animal for each antibody; the sections were within the injury epicentre, with an inter- spacing of 0.1 mm. For cell counting, images were captured at x40 magnification. For CCI studies, a minimum number of 200 fields of view (FoV) were captured per animal covering all 4 sections, with nuclei count of at least 3×10^4 nuclei. In addition, at least 30 fields were taken from the 4 sections along the lesion border (ipsi) for each animal and a similar number of fields were taken on the contralateral side (contra) of the brain (Fig. A.2). For rmTBI studies, a minimum number of 200 FoV were captured per animal covering all 4 sections, with a total of nuclei counts of at least 3×10^4 nuclei (Fig. A.3). For the γH2AX/53BP1 signal overlap, fields used for the quantification were taken at x60 magnification using the In Cell Analyser 6000 (INCA6000) Confocal System (Cytiva, Marlborough, United States).

All quantitative analyses were carried out using the In Cell Developer Toolbox v1.9.2 (Cytiva, Marlborough, United States), with custom-made protocols for each marker, using the built-in parameters selection tools. A cell was considered positive for a marker when the fluorescent signal co-localised with a nucleus by at least a 95% overlap. Results are expressed as a percentage of the total nuclei detected.

More images were taken, for some markers, at a magnification of 20× for an immunostaining 'heat map' generation (Fig. A.4). All images were captured using the In Cell Analyser 2200 (INCA2200) System (Cytiva, Marlborough, United States). For generating qualitative representations of p53, p21, p19ARF and GFAP staining within the tissue, which give more detail on the signal presence in various subregions, a scanned section was stitched together to form a composite image using ImageJ (ImageJ 1.53, National Institutes of Health, United States). More detail on the staining for p53 and p21 is provided in Appendix Fig. A.5 and Fig. A.6, respectively. Each area of the section was assessed manually for signal expression and highlighted if it was positive. Individual heat maps were generated for animals within a group and superimposing all heat maps generated the final heat map representing an experimental group (Fig. A.4). Heat maps reflect the location of the signal rather than intensity (number of cells expressing the signal) and darker areas indicate several animals within the group have an expression within the same region. Different colours were assigned to the various groups.

2.8. RT^2 Profiler PCR custom arrays

RNA was extracted from snap-frozen brain samples using the RNAeasy Plus Mini Kit (Cat. No. 74034; Qiagen, United Kingdom) according to the manufacturer's protocol. Samples were reverse transcribed into cDNA using the RT^2 First Strand Kit (Qiagen, United Kingdom). The starting amount of RNA used to generate cDNA was 1 μg per sample. Samples were analysed using custom made RT^2 Profiler PCR arrays (Qiagen, United Kingdom) (Table A.1). PCR plates were analysed using QuantStudio™ 7 FLEX system (QIAGEN, United States). Generated data were uploaded into the Qiagen data analysis web portal (https://dataanalysis2.qiagen.com/pcr). Generated fold regulation was used to present the data.

2.9. Statistical analysis

Statistical analysis was carried out using GraphPad Prism software (version 9; GraphPad Software Inc., La Jolla, CA). In most cases, data were plotted as median - minimum to maximum, showing all experimental points. For immunostaining data, the difference between the ipsilateral and contralateral hemispheres were compared using the Mann-Whitney Test, and the difference between the naïve, the sham, and the injured groups were compared using Kruskal–Wallis one-way analysis of variance. Friedman's test (two-way analysis of variance by ranks) was used to compare the behavioural data. All initial tests were followed by post-hoc tests for unequal sample sizes. The significance level was set at $p < 0.05$.

3. Results

3.1. Neurological function after single invasive and repetitive mild injury

The mNSS was used to assess changes in neurological function after injury by testing motor (muscle status, abnormal movement), sensory

Table 1
List of primary antibodies used in the experiments.

Marker	Antibody full name	Species	Company	Product ID	Dilution
Anti-p53	Anti-tumour protein P53	Rabbit	Insight Biotechnology, United States	GTX102965	1:150
Anti-p21	Anti-cyclin-dependent kinase inhibitor 1	Rabbit	Invitrogen, United States	14–6715-81	1:150
Anti- p16INK4a	Anti-cyclin-dependent kinase inhibitor 2 A	Rat	Abcam, United Kingdom	ab241543	1:150
Anti- p19ARF	Anti-ARF tumour suppressor	Rat	Novus Biological, United States	NB200–169	1:150
Anti-γH2AX	Anti-phosphorylated H2A histone family member X	Mouse	Merck KGaA, Germany	05–636	1:500
Anti-53BP1	Anti-tumour suppressor p53-binding protein 1	Rabbit	Cambridge Bioscience, United Kingdom	A300-273 A	1:1600
Anti-Iba-1	Anti-ionized calcium-binding adaptor molecule 1	Rabbit	FUJIFILM Wako Pure Chemical Corporation, Japan	019–19,741	1:250
Anti-P2Y12	Anti-purinergic receptor P2Y, G-protein coupled 12	Rabbit	AnaSpec, United States	55043 A-ANA	1:250
Anti-GFAP	Anti-glial fibrillary acidic protein	Rabbit	Agilent Technologies, United States	Z033429–2	1:800
Anti-8-oxo	Anti-8-hydroxyguanine	Mouse	QED bioscience, Inc., United States	ABIN190029	1:500

(visual, tactile and proprioceptive) and reflex responses. The CCI group showed significant impairments at 1 day and 3 days after injury (Fig. A.1, C) and there was a gradual decrease in mNSS scores during the five days of testing. In the Cranio group, animals showed a significant impairment 1 day after injury (**$p = 0.0044$, Fig. A.1, C), followed by a gradual recovery (*$p = 0.05$). In the rmTBI experiment, animals' scores in all groups were below 4 (ranging between 0 and 3), i.e. a normal or minimum impairment score (Fig. A.1, D). There was no statistically significant difference between the groups in the rmTBI experiment, during the 6 days of testing.

3.2. Histological assessment of cellular senescence

The markers investigated, related to DNA damage response (DDR)-induced senescence, included p53, p21, p19ARF, and γH2AX/53BP1 co-localization. Another marker was p16INK4a, related to chromatin changes and senescence-associated heterochromatin foci (SAHF).

Representative images of p53 staining, the quantification of the number of p53-positive cells, and a heat map representation of areas that express the signal are shown in Fig. 1. Overall, the CCI experiment (Fig. 1 B [a,b]) showed a high expression of p53 at 5 days post-injury (dpi) in the Cranio (median = 23.3%) and the CCI (median = 16.3%) groups, when compared to the naïve group (median = 1.9%) and this was statistically significant ($p < 0.0001$). There were differences between the CCI group vs. the naïve group (*$p = 0.0286$), the CCI group vs. the Cranio group (*$p = 0.0159$), and the Cranio group vs. the naïve group (*p = 0.0159). There was no statistically significant difference between the ipsilateral and contralateral hemispheres ($p = 0.5476$). At

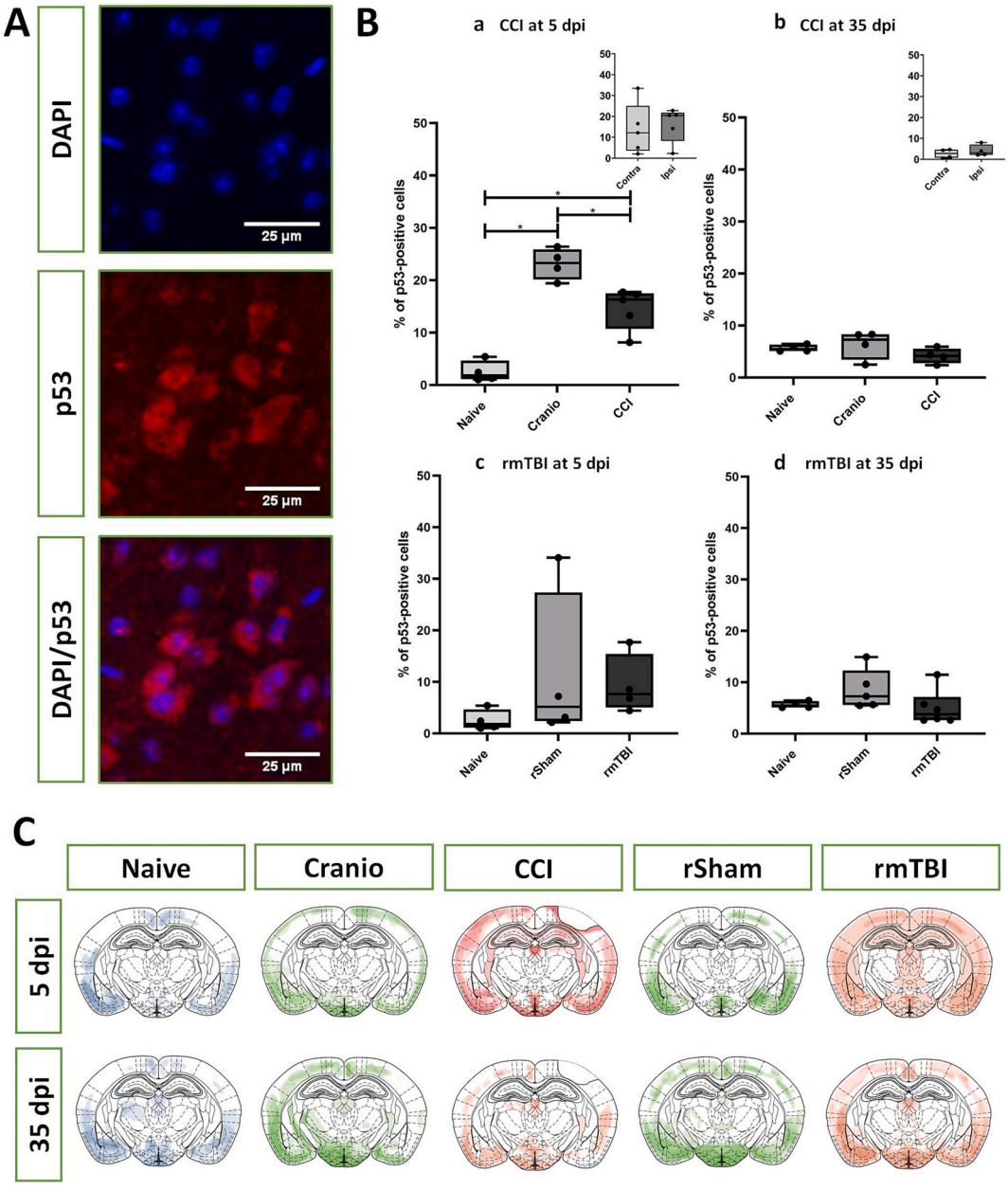

Fig. 1. Immunofluorescence staining for p53. (A) Representative images of p53 staining, (B) The quantification of p53 in the CCI and rmTBI experiments, [a] CCI at 5 dpi, [b] CCI at 35 dpi, [c] rmTBI at 5 dpi, [d] rmTBI at 35 dpi, (C) Heat map representation of areas that express the signal. Results represent the median, minimum and maximum. Data were analysed using the Kruskal-Wallis test followed by the Dunn-Bonferroni test; *$P < 0.05$. For CCI- At 5 dpi: 4 animals for naive, 4 animals for Cranio and 5 animals for CCI. At 35 dpi: 4 animals for naive, 4 animals for Cranio and 4 animals for CCI. For rmTBI - At 5 dpi: 4 animals for naive, 4 animals for rSham and 4 animals for rmTBI. At 35 dpi: 4 animals for naive, 5 animals for rSham and 6 animals for rmTBI.

35 dpi, there was no difference between the groups ($p = 0.2118$) or between the ipsilateral and contralateral hemispheres ($p = 0.6857$). In the rmTBI experiment, there was no statistically significant difference in the expression of p53 (Fig. 1 B [c,d]) between the groups at 5 dpi ($p = 0.1042$) and 35 dpi ($p = 0.1253$).

For p21, Fig. 2 shows the immunostaining, quantification of signal, and heat maps representing spread of the signal. In the CCI experiment (Fig. 2 B [a,b]), there was no statistically significant difference between the groups at 5 dpi ($p = 0.7681$) as well as between the ipsilateral and contralateral hemispheres ($p = 0.2$). However, there was a difference in expression between the groups at 35 dpi ($p = 0.0403$), specifically, between the naïve group vs the CCI group ($^*p = 0.0286$) – with a higher level in the naïve group. There was no statistically significant difference between the ipsilateral and contralateral hemispheres ($p = 0.6857$). In the rmTBI experiment (Fig. 2 B [c,d]), there was no statistically significant difference between the groups at 5 dpi ($p = 0.1567$). However, there was a clear difference in expression between the groups at 35 dpi ($p = 0.0009$), specifically, between the naïve group vs the rSham group ($^*p = 0.0159$), and the naïve group vs the rmTBI group ($^{**}p = 0.0095$), with injury leading to lower levels.

The analysis of immunostaining for p19ARF (quantification of signal and heat map representation), shown in Fig. 3, indicates that in the CCI experiment (Fig. 3 B [a,b]), there was a clear difference between the groups at 5 dpi ($p < 0.0001$), specifically, between the CCI group vs. the naïve group ($^*p = 0.0159$), the CCI group vs. the Cranio group ($^*p = 0.0159$) – with a higher level in the Cranio group, and the Cranio group vs. the naïve group ($^*p = 0.0286$). In addition, there was a significant difference between the ipsilateral and contralateral hemispheres ($^{**}p =$

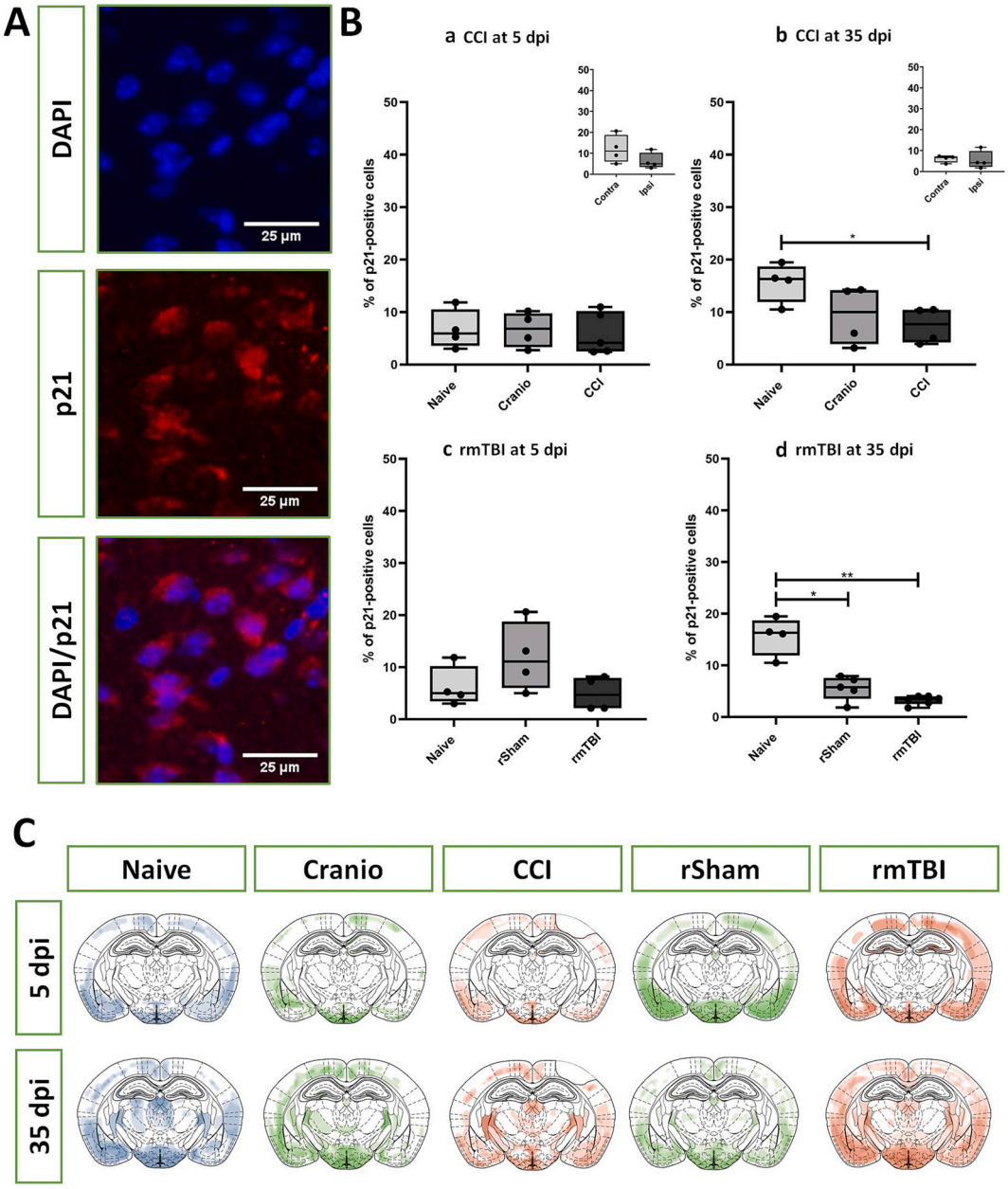

Fig. 2. Immunofluorescence staining for p21. (A) Representative images of p21 staining, (B) The quantification of p21 in the CCI and rmTBI experiments, [a] CCI at 5 dpi, [b] CCI at 35 dpi, [c] rmTBI at 5 dpi, [d] rmTBI at 35 dpi, (C) Heat map representation of areas that express the signal. Results represent the median, minimum and maximum. Data were analysed using the Kruskal-Wallis test followed by the Dunn-Bonferroni test; $^*P < 0.05$, $^{**}P < 0.01$. For CCI - At 5 dpi: 4 animals for naive, 4 animals for Cranio and 5 animals for CCI. At 35 dpi: 4 animals for naive, 4 animals for Cranio and 4 animals for CCI. For rmTBI - At 5 dpi: 4 animals for naive, 4 animals for rSham and 4 animals for rmTBI. At 35 dpi: 4 animals for naive, 5 animals for rSham and 6 animals for rmTBI.

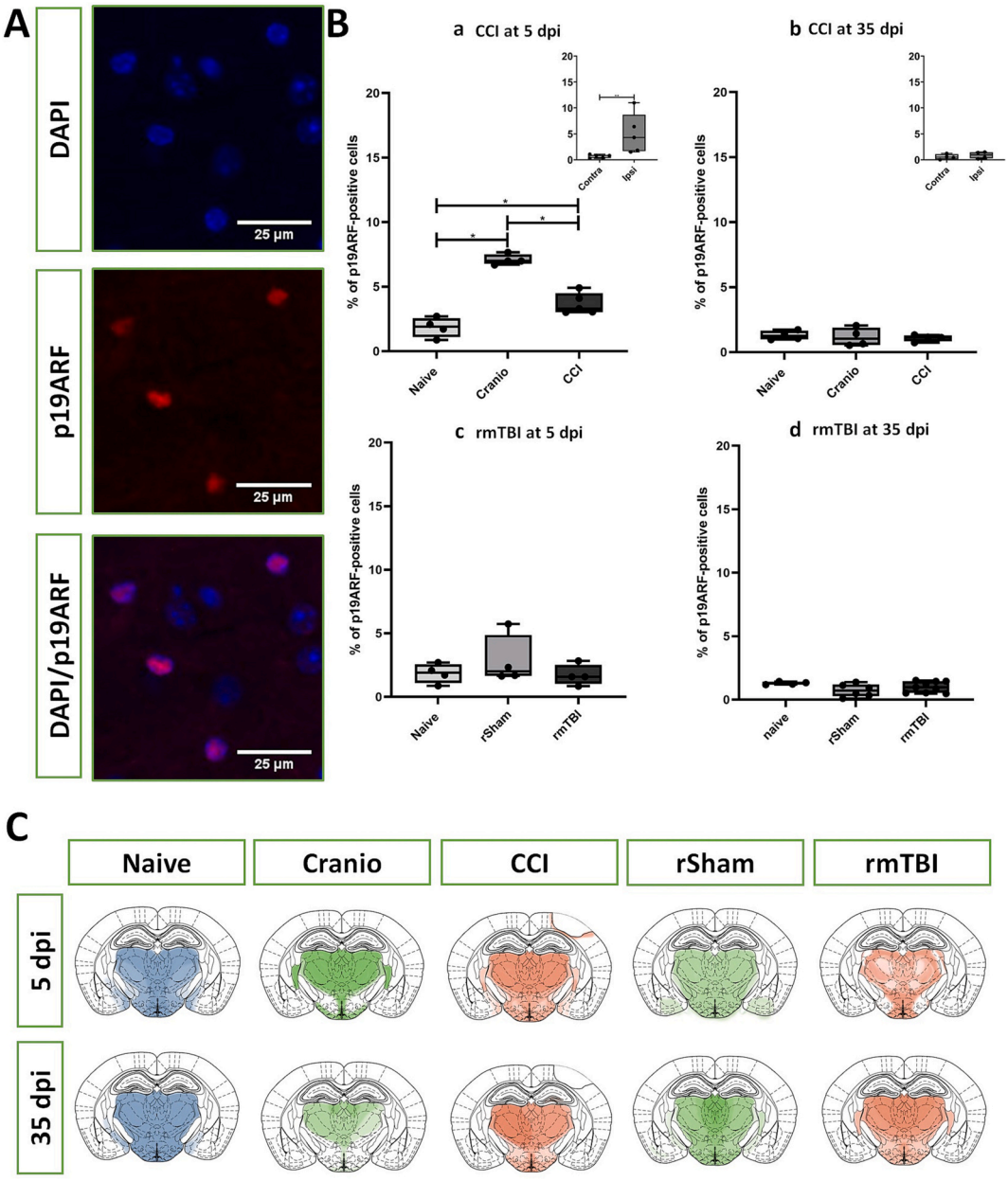

Fig. 3. Immunofluorescence staining for p19ARF. (A) Representative images of p19ARF staining, (B) The quantification of p19ARF in the CCI and rmTBI experiments, [a] CCI at 5 dpi, [b] CCI at 35 dpi, [c] rmTBI at 5 dpi, [d] rmTBI at 35 dpi, (C) Heat map representation of areas that express the signal. Results represent the median, minimum and maximum. Data were analysed using the Kruskal-Wallis test followed by the Dunn-Bonferroni test; $*P < 0.05$, $**P < 0.01$. For CCI - At 5 dpi: 4 animals for naive, 4 animals for Cranio and 5 animals for CCI. At 35 dpi: 4 animals for naive, 4 animals for Cranio and 4 animals for CCI. For rmTBI - At 5 dpi: 4 animals for naive, 4 animals for rSham and 4 animals for rmTBI. At 35 dpi: 4 animals for naive, 8 animals for rSham and 9 animals for rmTBI.

0.0079). At 35 dpi, there was no significant difference between the groups ($p = 0.8400$) or the ipsilateral and contralateral hemispheres ($p = 0.4857$). In the rmTBI, there was no difference between the groups at 5 dpi ($p = 0.4675$) and 35 dpi ($p = 0.7863$). The heat map representation indicated a predominant subcortical signal across all groups.

We also investigated γH2AX/53BP1 co-localization (Fig. 4). γH2AX is a marker of double strand break and 53BP1 is a DDR factor. The co-localization of these two proteins signifies an irreversible DNA double-strand break or double foci (DF), and this is a definitive marker of cellular senescence. In the CCI experiment (Fig. 4 C [a,b]), analysis showed a significant difference between the groups at 5 dpi ($p = 0.0014$), specifically, between the CCI group vs. the naïve group ($*p = 0.0317$) and the Cranio group vs. the naïve group ($*p = 0.0286$). Additionally, there was no significant difference between the ipsilateral and contralateral hemispheres ($p = 0.8413$). At 35 dpi, there was no significant difference between the groups ($p = 0.1619$) and between the ipsilateral and contralateral hemispheres ($p > 0.9999$). In the rmTBI, results showed no difference between the groups at 5 dpi ($p = 0.7061$) and 35 dpi ($p = 0.2471$) (Fig. 4 C [c,d]).

For the analysis of p16INK4a, Fig. 5 shows representative images of staining and quantification. In the CCI experiment (Fig. 5 B [a,b]), the expression of p16INK4a at 5 dpi was higher in the CCI group (median = 0.61%) and the Cranio group (median = 1.03%) when compared to the naïve group (median = 0.29%) and this was statistically significant ($p = 0.0123$). Specifically, between the CCI group vs. the naïve group ($*p = 0.0328$) and the Cranio group vs. the naïve group ($*p = 0.0286$). There was no significant difference between the ipsilateral and contralateral hemispheres ($p = 0.0556$). At 35 dpi, there was no statistically

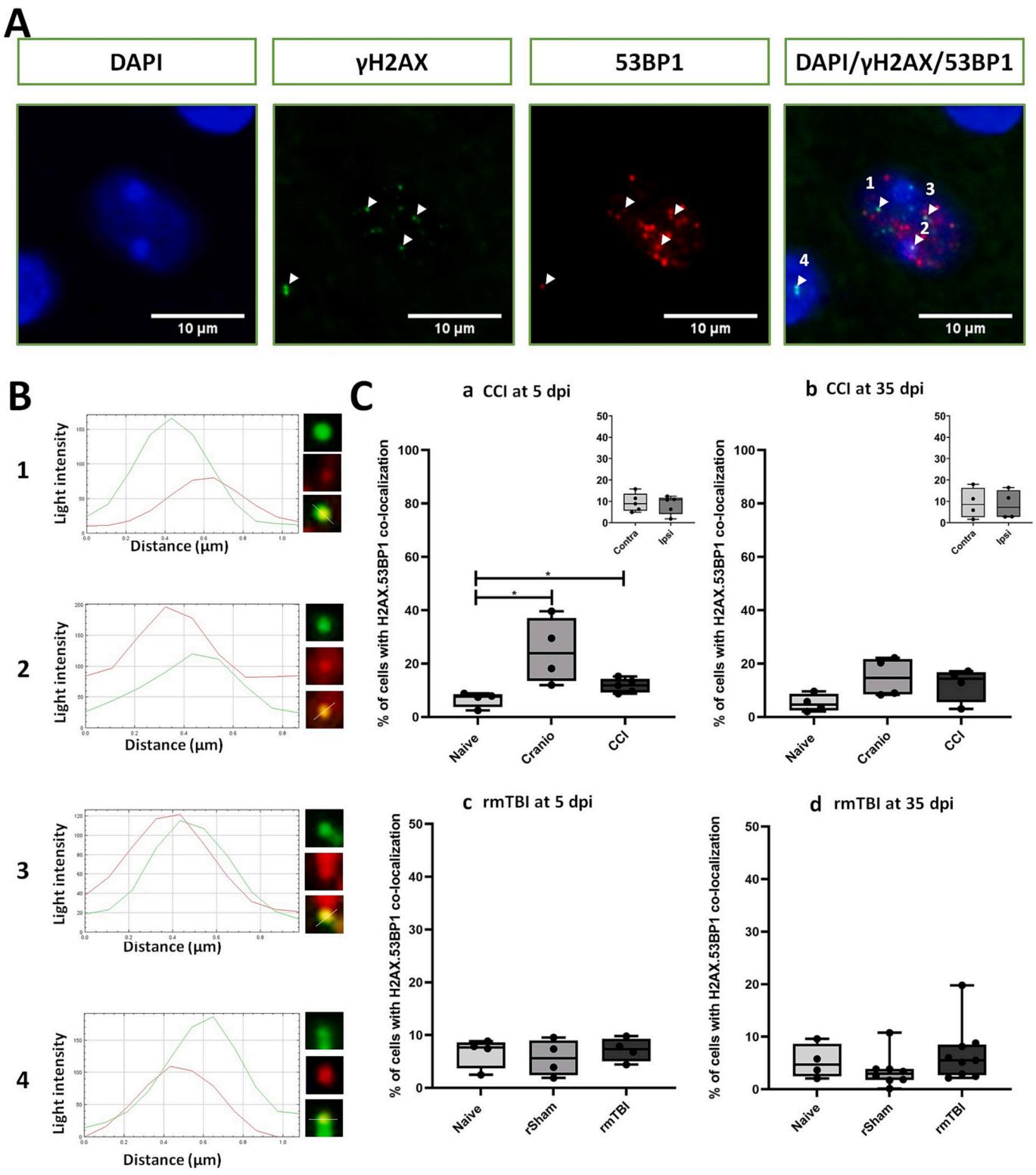

Fig. 4. Immunofluorescence staining for γH2AX and 53BP1 co-localization. (A) The expression of γH2AX and 53BP1 in a nucleus, the arrow demonstrates a double focus (DF), (B) The histogram displays the overlap of γH2AX and 53BP1 foci, (C) The quantification of γH2AX/53BP1 co-localization in the CCI and rmTBI experiments, [a] CCI at 5 dpi, [b] CCI at 35 dpi, [c] rmTBI at 5 dpi, [d] rmTBI at 35 dpi. Results represent the median, minimum and maximum. Data were analysed using the Kruskal-Wallis test followed by the Dunn-Bonferroni test; $^{*}P < 0.05$, $^{**}P < 0.01$. For CCI - At 5 dpi: 4 animals for naive, 4 animals for Cranio and 5 animals for CCI. At 35 dpi: 4 animals for naive, 4 animals for Cranio and 4 animals for CCI. For rmTBI - At 5 dpi: 4 animals for naive, 4 animals for rSham and 4 animals for rmTBI. At 35 dpi: 4 animals for naive, 8 animals for rSham and 9 animals for rmTBI).

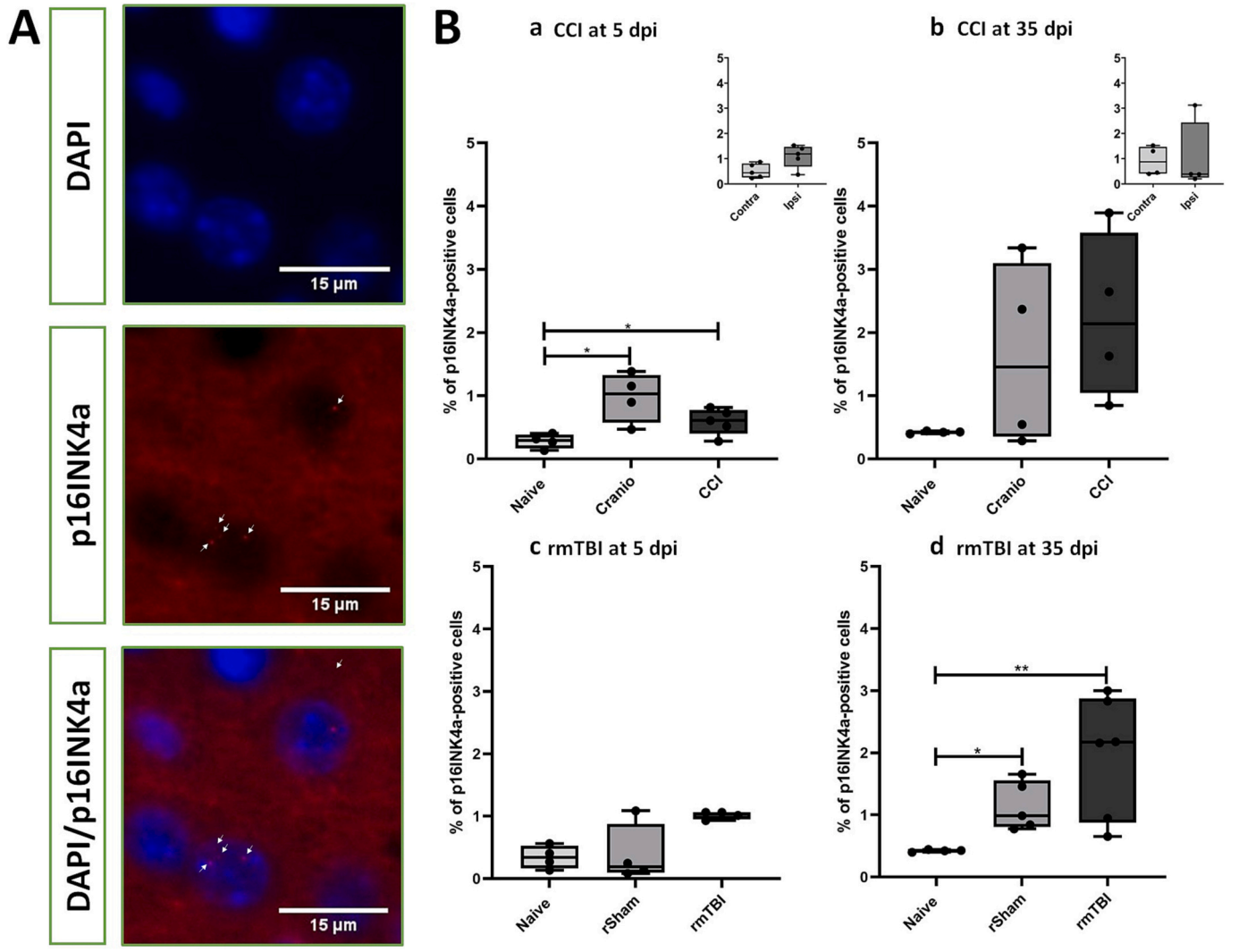

Fig. 5. Immunofluorescence staining for p16INK4a. (A) Representative images of p16INK4a staining, (B) The quantification of p16INK4a in the CCI and rmTBI experiments, [a] CCI at 5 dpi, [b] CCI at 35 dpi, [c] rmTBI at 5 dpi, [d] rmTBI at 35 dpi. Results represent the median, minimum and maximum. Data were analysed using the Kruskal-Wallis test followed by the Dunn-Bonferroni test; $^{*}P < 0.05$, $^{**}P < 0.01$. For CCI - At 5 dpi: 4 animals for naive, 4 animals for Cranio and 5 animals for CCI. At 35 dpi: 4 animals for naive, 4 animals for Cranio and 4 animals for CCI. For rmTBI - At 5 dpi: 4 animals for naive, 4 animals for rSham and 4 animals for rmTBI. At 35 dpi: 4 animals for naive, 4 animals for rSham and 6 animals for rmTBI.

significant difference between the groups ($p = 0.0741$). In addition, there was no significant difference between the ipsilateral and contralateral hemispheres ($p = 0.3429$). In the rmTBI experiment (Fig. 5 B [c, d]), there was no statistically significant difference in the expression of p16INK4a between the groups ($p = 0.1297$) but there was a tendency of increased expression in the rSham and rmTBI groups. Interestingly, the trend continued at 35 dpi and it was statistically significant ($p = 0.0029$); the naïve group vs. the rSham group ($^{*}p = 0.0159$) and the naïve group vs. the rmTBI group ($^{**}p = 0.0095$).

3.3. Assessment of the neuroinflammatory response

Different markers were used to assess changes associated with the neuroinflammatory response after TBI. We investigated markers related to microglia - e.g. Iba-1 (microglia/macrophages) and P2Y12 (general marker of microglia in the healthy brain), and astrocytes (GFAP). In the CCI experiment (Fig. 6 B [a,b]), there was increased expression in Iba-1 at 5 dpi ($^{**}p = 0.0025$) between the CCI group vs. the naïve group ($^{*}p = 0.0159$) and the CCI group vs. the Cranio group ($^{**}p = 0.0079$). There was a statistically significant difference between the ipsilateral and contralateral hemispheres ($^{**}p = 0.0079$). At 35 dpi, statistical analysis showed no significant difference between the groups ($p = 0.9945$) and between the ipsilateral and contralateral hemispheres ($p = 0.1143$). In the rmTBI experiment (Fig. 6 B [c,d]), there were no significant differences at 5 dpi ($p = 0.0545$) and 35 dpi ($p = 0.1465$).

For the P2Y12 signal (Fig. 7), after the CCI experiment there was an increase in expression overall at 5 dpi ($p = 0.0395$), particularly, between the CCI group vs. the naïve group ($^{*}p = 0.0159$). There was no significant difference between the ipsilateral and contralateral hemispheres ($p = 0.3095$). At 35 dpi, P2Y12 expression was significantly lower ($p = 0.0132$) - between the CCI group vs. the naïve group ($^{*}p = 0.0286$) and the Cranio group vs. the naïve group ($^{*}p = 0.0286$). There was no significant difference between the ipsilateral and contralateral hemispheres ($p = 0.6857$). In the rmTBI experiment, there was no difference in expression between the groups at 5 dpi ($p = 0.4184$) and 35 dpi ($p = 0.1886$).

For GFAP (Fig. 8), the results of the CCI experiment (Fig. 8 B [a,b]) showed a significant difference between the groups at 5 dpi ($p = 0.0002$). There were differences between the CCI group vs. the naïve group ($^{*}p = 0.0159$), the Cranio group vs. the naïve group ($^{*}p = 0.0317$), and the CCI group vs. the Cranio group ($^{*}p = 0.0159$). In addition, there was a statistically significant difference between the

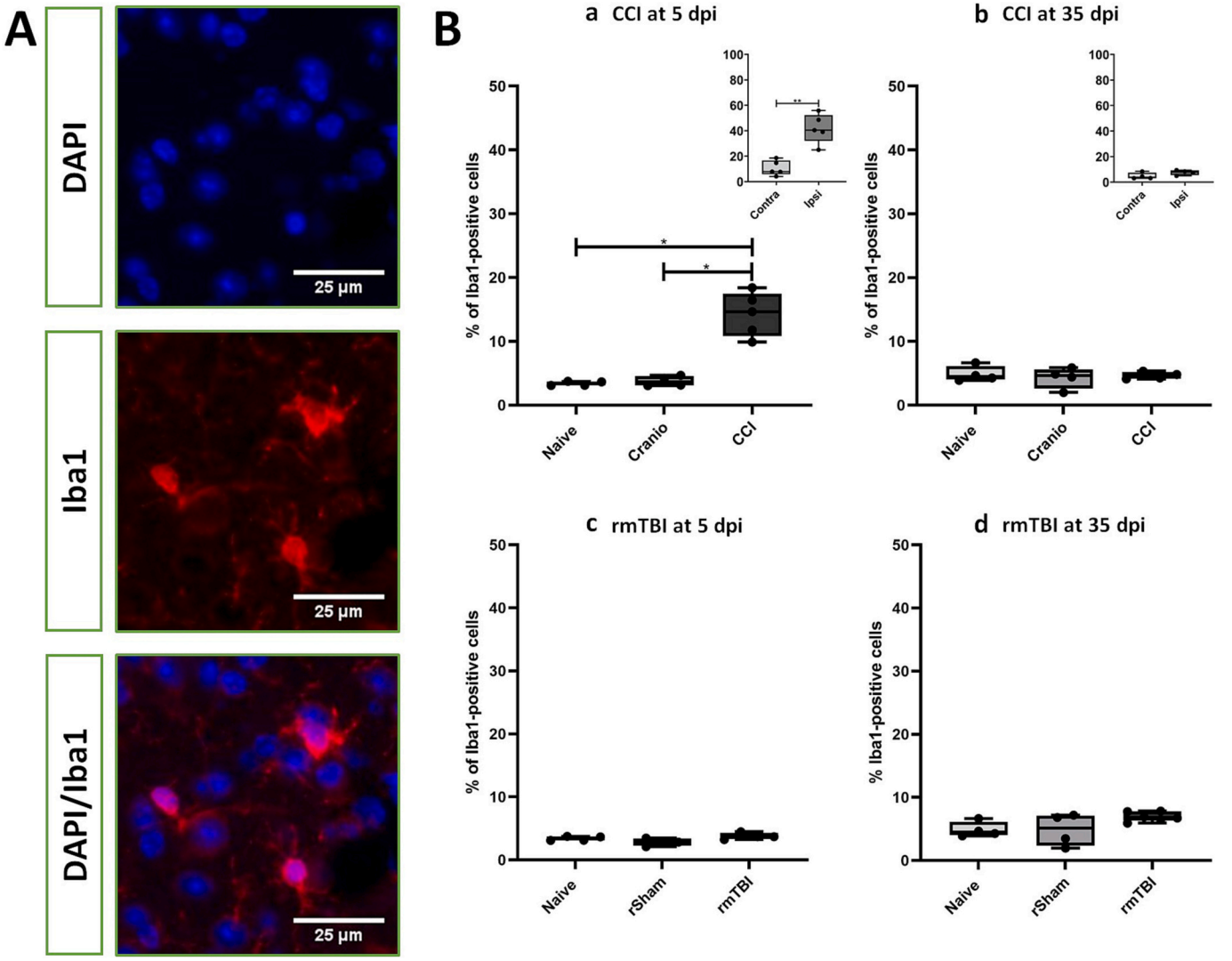

Fig. 6. Immunofluorescence staining for Iba1. (A) Representative images of Iba1 staining, (B) The quantification of Iba1 in the CCI and rmTBI experiments, [a] CCI at 5 dpi, [b] CCI at 35 dpi, [c] rmTBI at 5 dpi, [d] rmTBI at 35 dpi. Results represent the median, minimum and maximum. Data were analysed using the Kruskal-Wallis test followed by the Dunn-Bonferroni test; $^{*}P < 0.05$, $^{**}P < 0.01$. For CCI - At 5 dpi: 4 animals for naive, 4 animals for Cranio and 5 animals for CCI. At 35 dpi: 4 animals for naive, 4 animals for Cranio and 4 animals for CCI. For rmTBI - At 5 dpi: 4 animals for naive, 4 animals for rSham and 4 animals for rmTBI. At 35 dpi: 4 animals for naive, 4 animals for rSham and 6 animals for rmTBI.

ipsilateral and contralateral hemispheres (**$p = 0.0079$). At 35 dpi, the analysis showed a significant difference between the groups ($p = 0.0300$), particularly between the Cranio group vs. the CCI group (*$p = 0.0286$). Also, there was a statistically significant difference between the ipsilateral and contralateral hemispheres (*p = 0.0286). In the rmTBI experiment (Fig. 8 B [c,d]), there were no differences induced by the injury at 5 dpi ($p = 0.8400$) and 35 dpi ($p = 0.6827$).

We also investigated a marker of oxidative stress, as this process is closely linked to the induction of senescence. 8-hydroxyguanosine (8-oxo), an oxidative derivative of guanosine, is a reflection of nucleic acid oxidative stress (Fig. 9). In the CCI experiment, there was a significant difference in the expression of 8-oxo ($p = 0.0021$) - specifically, between the CCI group vs. the naïve group (*$p = 0.0159$) and the Cranio group vs. the naïve group (*p = 0.0286). There was no difference between the ipsilateral and contralateral hemispheres ($p = 0.4206$). At 35 dpi, there was a statistically significant difference overall ($p = 0.0403$). The expression of 8-oxo was not different in the ipsilateral vs. the contralateral hemisphere ($p = 0.4857$). In the rmTBI experiment, the quantification of the signal showed no statistically significant difference between the groups at 5 dpi ($p = 0.0741$) and 35 dpi ($p = 0.2294$).

3.4. Gene expression and cellular senescence

To further investigate the role of cellular senescence in TBI, we carried out an analysis using PCR arrays, on a set of selected genes (Table A.1). In the CCI experiment, the analysis revealed several changes between naïve, Cranio, the contralateral hemisphere (Contra) and the ipsilateral hemisphere (Ipsi) of the CCI group, at both time points (Fig. 10; Table 2). At 5 dpi, three genes were significantly changed between the Ipsi group and the naïve group (increases in *Il1a*, *Gfap*, and decreases in *Brca1*), whereas in the contralateral hemisphere, there were no changes. At 35 dpi, nine genes which were significantly changed between the Ipsi group and the naïve group (increases in *Il1a*, *Ccl8*, *Ccl3*, *GFAP*, and decreases in*Cdkn1a*, *Gadd45a*, *Casp9*, *Map2* and *Dpysl2*). In the contralateral hemisphere, ten genes were significantly changed (increases in *Ifnb1*, *Trp63*, *Ccnb1*, *Csf2*, *Ccl26*, *Cxcl2* and *Fas*, and decreases in *Wrn*, *Casp9*, and *Map2*). In the Cranio group, two genes were significantly changed vs. naïve at 5 dpi (increases in *Ccnb1* and *Casp3*), and five were changed at 35 dpi (increases in *Csf2*, *Ccl26*, *Cxcl2*, and decreases in *Casp9*, and *Gfap*).

In the rmTBI experiment, the analysis revealed minor changes

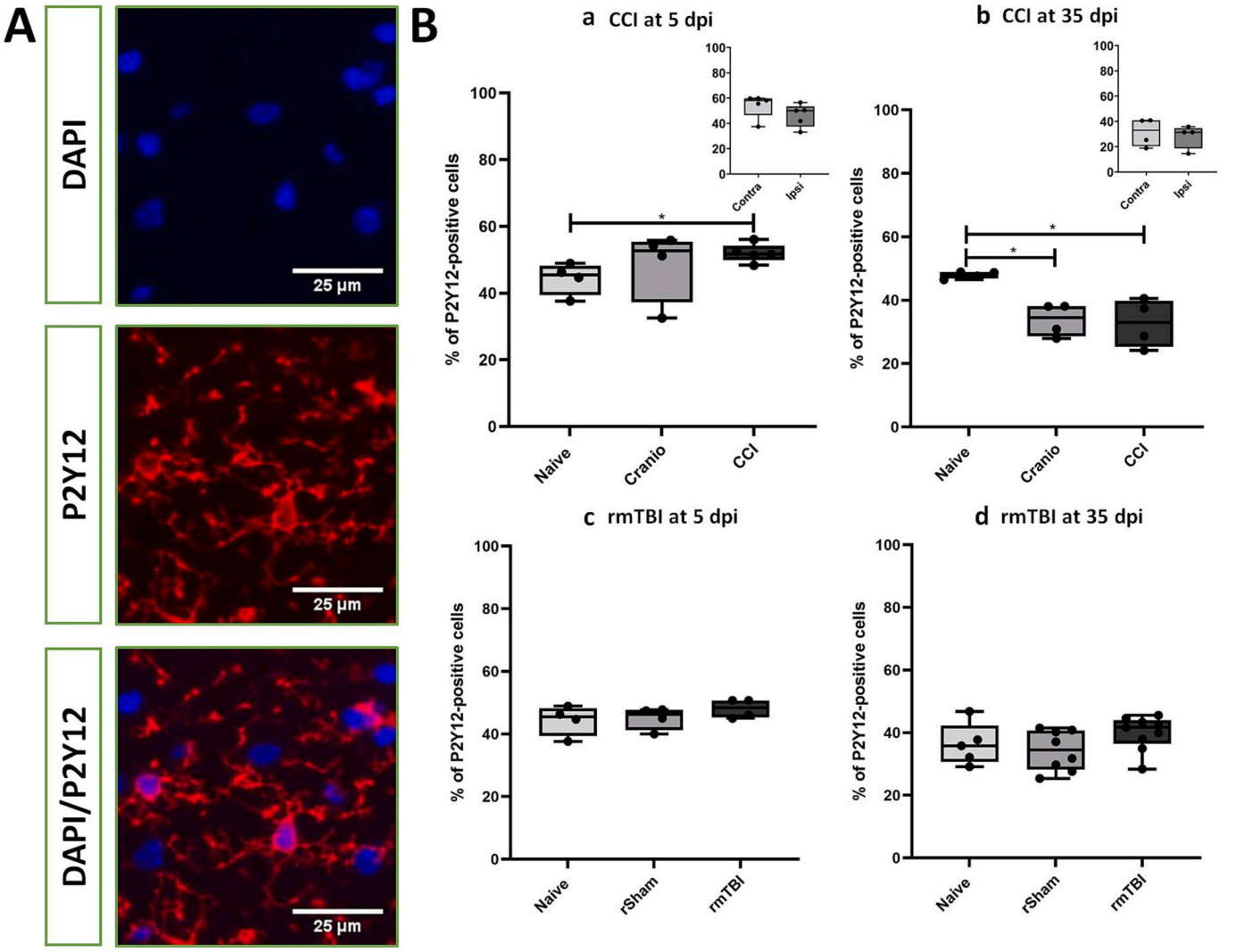

Fig. 7. Immunofluorescence staining for P2Y12. (A) Representative images of P2Y12 staining, (B) The quantification of P2Y12 in the CCI and rmTBI experiments, [a] CCI at 5 dpi, [b] CCI at 35 dpi, [c] rmTBI at 5 dpi, [d] rmTBI at 35 dpi. Results represent the median, minimum and maximum. Data were analysed using the Kruskal-Wallis test followed by the Dunn-Bonferroni test; $*P < 0.05$. For CCI - At 5 dpi: 4 animals for naive, 4 animals for Cranio and 5 animals for CCI. At 35 dpi: 4 animals for naive, 4 animals for Cranio and 4 animals for CCI. For rmTBI - At 5 dpi: 4 animals for naive, 4 animals for rSham and 4 animals for rmTBI. At 35 dpi: 4 animals for naive, 7 animals for rSham and 8 animals for rmTBI.

between the naïve group vs the rmTBI and some changes between the naïve group and the rSham group (Fig. 10, Table 3). There were no genes which were significantly changed between the rmTBI group and the naïve group at 5 dpi and 35 dpi. In the rSham group, one gene was significantly increased at 5 dpi (*Ccl8*), but interestingly, twenty genes were significantly increased at 35 dpi, including *Mdm2*, *Atm*, *Rb1*, *Ccna2*, *Cdkn1b*, *Ifnb1*, *Cdk6*, *Trp53bp1*, *Trp63*, *Rad51*, *Wrn*, *Csf2*, *Egf*, *Ccl26*, *Ccl3*, *Mmp9*, *Mif*, *Fgf2*, *Fas*, and *Cdk5*.

To further analyse results from the GeneGlobe analysis (Fig. 10), data were uploaded to QIAGEN Ingenuity Pathway Analysis (IPA) to align all genes (detected by qPCR or predicted) with their databases, and identify pathways activated/inactivated. Datasets of the ipsilateral and contralateral hemispheres and the craniotomy group showed a list of pathways which were predicted to have a significant change based on their z-score (Table A.2 and Table A.3). CCI was associated with pathways linked to the DNA damage response, cellular senescence and also immune system response to injury. For datasets from the rmTBI experiment, there was association with cellular homeostasis and apoptosis, DNA damage signalling, DNA damage response and immune system response.

4. Discussion

Children, adolescents and young adults are affected by TBI, and there are few clinical studies on moderate/severe brain injuries in children and adolescents when compared to other age groups (Kennedy et al., 2022). Effects of a moderate to severe impact may persist for many years (Cole et al., 2008). The assessment of injury outcomes is especially important given the brain is still in the developing stage (Ewing-Cobbs et al., 2006; Rosema et al., 2012). Negative outcomes include behavioural disorders, impaired intellectual development and poorer social function. Furthermore, children and adolescents are also significantly exposed to repeated mild brain injuries, for example repeated concussion episodes during contact sports (McAllister and McCrea, 2017). Repeated concussions have been recognised as a major cause of neurodegenerative conditions such as chronic traumatic encephalopathy (CTE) (Mckee and Daneshvar, 2015; Montenigro et al., 2015). More recently, the concept of subconcussion has also emerged (McKee and Daneshvar, 2015; Montenigro et al., 2015), with evidence indicating that even in the absence of immediate clinical signs, the brain tissue activates an injury response which may have long-lasting consequences (Hirad et al., 2019).

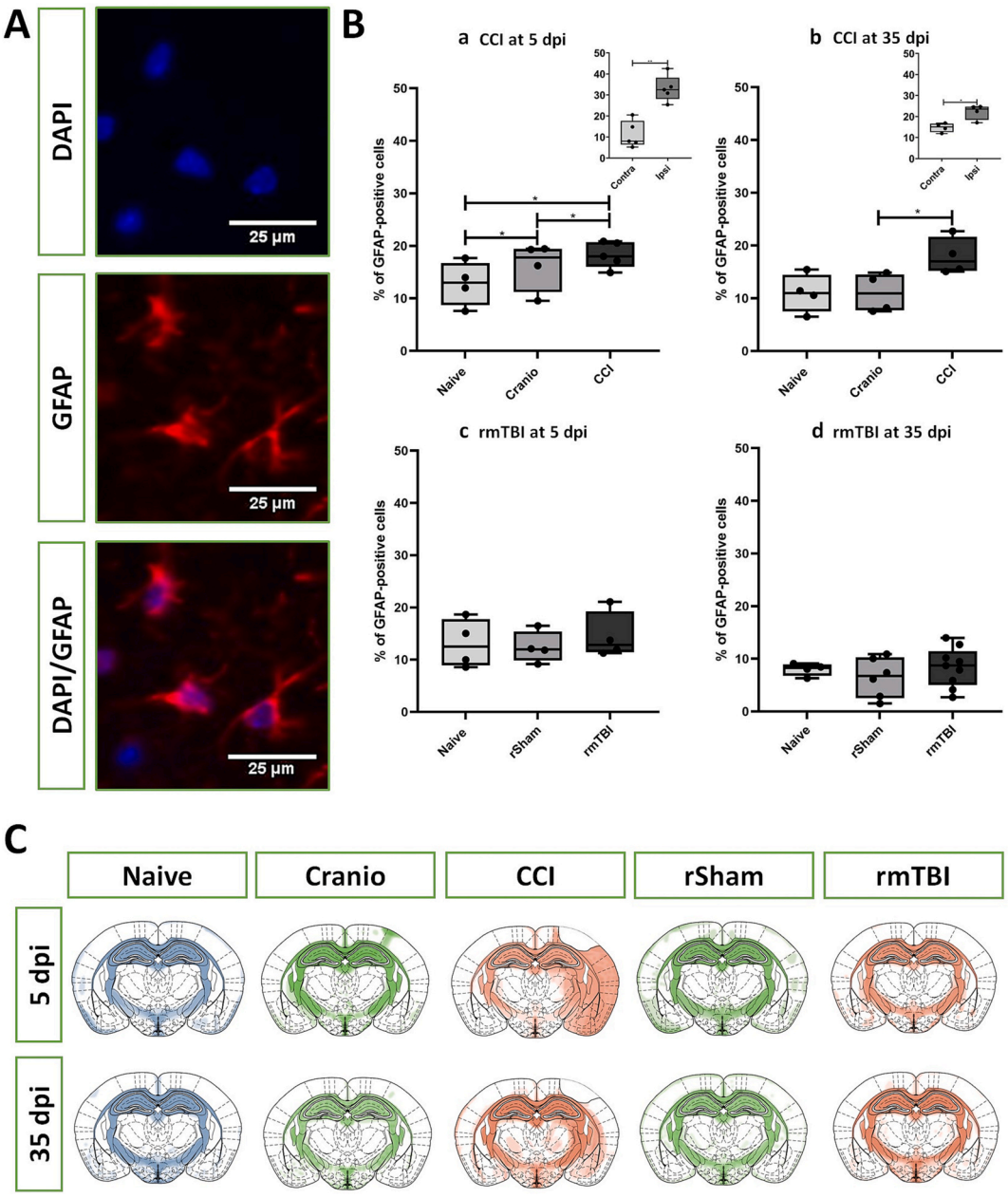

Fig. 8. Immunofluorescence staining for GFAP. (A) Representative images of GFAP staining, (B) The quantification of GFAP in the CCI and rmTBI experiments, [a] CCI at 5 dpi, [b] CCI at 35 dpi, [c] rmTBI at 5 dpi, [d] rmTBI at 35 dpi, (C) Heat map representation of areas that express the signal. Results represent the median, minimum and maximum. Data were analysed using the Kruskal-Wallis test followed by the Dunn-Bonferroni test; $^{*}P < 0.05$, $^{**}P < 0.01$. For CCI - At 5 dpi: 4 animals for naive, 4 animals for Cranio and 5 animals for CCI. At 35 dpi: 4 animals for naive, 4 animals for Cranio and 4 animals for CCI. For rmTBI - At 5 dpi: 4 animals for naive, 4 animals for rSham and 4 animals for rmTBI. At 35 dpi: 4 animals for naive, 6 animals for rSham and 9 animals for rmTBI.

Here we focus on two different modes of injury: a moderate invasive unilateral single injury and a repetitive mild injury, and investigate whether the injury in the immature brain activates a cellular senescence response, as has been shown to occur in adult brain already in the acute phase post-injury (Katano et al., 2000; Ritzel et al., 2019; Schwab et al., 2021; Schwab et al., 2022; Tominaga et al., 2019).

The juvenile mouse developmental stage of animals in this study (around 30–35 day-old at the time of injury), would represent a late childhood, pre-teen stage in humans, according to Dutta and Sengupta (2016), whose estimate is that at a mouse pre-pubertal stage, 3.65 mouse days are equivalent to 1 human year.

The relationship between injury severity and the level of neurological impairment is well established in clinical studies (Cappa et al., 2011) and animal models (Tsenter et al., 2008). A gradual recovery after injury is observed in children and young adults who sustain a mild or a moderate/severe injury (Kuhtz-Buschbeck et al., 2003; Rosenbaum et al., 2020), as well as in animal studies (Tsenter et al., 2008). Our assessment of juvenile animals with CCI showed a moderate sensorimotor behavioural impairment after injury, which resolved with time. In contrast, rmTBI animals showed overall no impairment when assessed using mNSS. This indicates that it is likely that we had induced the equivalent of a human subconcussive state, similar to what was reported in the adult rat by Lavender and collaborators (Lavender et al., 2020).

Microglia and astrocytes play an important role in the pathophysiology of TBI, particularly in the complex neuroinflammatory response post-injury (Donat et al., 2017; Gottlieb et al., 2022; Mira et al., 2021; Yu et al., 2021; Yuan and Wu, 2022). Understanding how this immune neuroinflammation response evolves post-injury could shed light on its

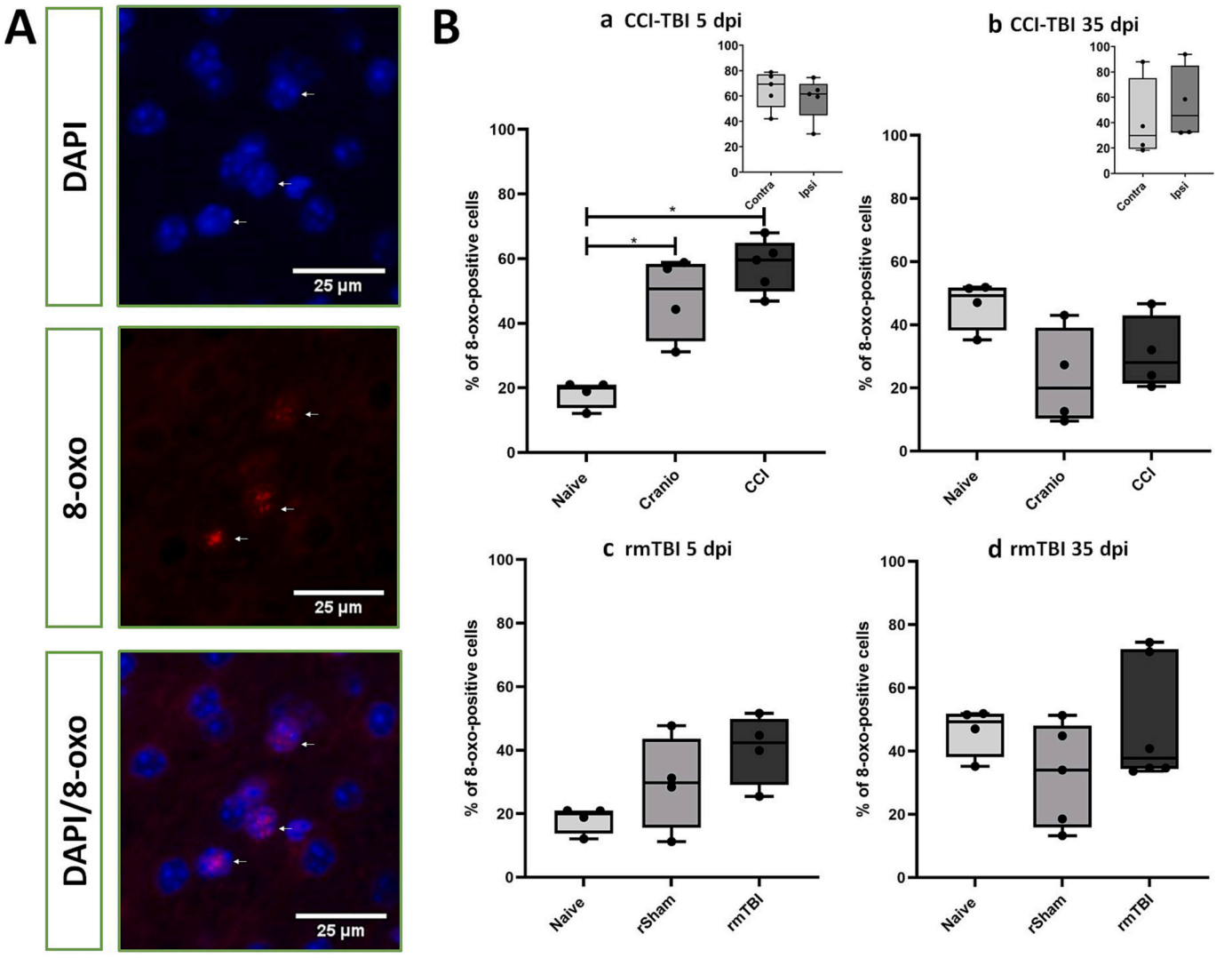

Fig. 9. Immunofluorescence staining for 8-hydroxyguanosine (8-oxo). (A) Representative images of 8-oxo staining, (B) The quantification of 8-oxo in the CCI and rmTBI experiments, [a] CCI at 5 dpi, [b] CCI at 35 dpi, [c] rmTBI at 5 dpi, [d] rmTBI at 35 dpi. Results represent the median, minimum and maximum. Data were analysed using the Kruskal-Wallis test followed by the Dunn-Bonferroni test; $^{*}P < 0.05$. For CCI - At 5 dpi: 4 animals for naive, 4 animals for Cranio and 5 animals for CCI. At 35 dpi: 4 animals for naive, 4 animals for Cranio and 4 animals for CCI. For rmTBI - At 5 dpi: 4 animals for naive, 4 animals for rSham and 4 animals for rmTBI. At 35 dpi: 4 animals for naive, 5 animals for rSham and 6 animals for rmTBI.

potential beneficial or pathogenic impact on the immature brain. Therefore, we focused on the reaction of microglia (measured using Iba1 and P2Y12) and astrocytes (assessed through GFAP) in the two injury models.

The analysis of CCI tissue at the early time point, showed clear reactive astrogliosis and reactive microglia/macrophages, as well as increased oxidative stress – which confirms the induction of a more intense injury. Later on, reactive astrogliosis persisted, with no significant differences in reactive microglia/macrophages or oxidative stress. This is similar to our observations after CCI in adult mice (Thau-Zuchman et al., 2019; Thau-Zuchman et al., 2020; Thau-Zuchman et al., 2021). Some studies have reported the persistence of reactive astrocytes and microglia in the subacute phase after injury or even at a much longer, chronic time post-injury (>6 months) (Ertürk et al., 2016; Fenn et al., 2014; Janatpour et al., 2019). However, one study in juvenile rats with CCI reported no persistence of reactive microglia (Smith et al., 2019). In our study, after rmTBI in juveniles the injured tissue showed no reactive astrogliosis or reactive microglia/macrophages in the acute phase. The oxidative stress marker showed a trend towards increased expression in the acute phase, with no change in the subacute phase. These observations are different from other studies which modelled rmTBI in juveniles or adults (using various different protocols for induction of injuries), which showed that astrogliosis and microgliosis can be detected in some cases in the subacute and chronic phases after injury (Chen et al., 2017; Luo et al., 2014). For example, a study in a closed head injury model that mimicked acceleration and deceleration injury, detected reactive astrocytes (GFAP) and microglia (Iba1) up to 6 months after repetitive injury (3 impacts with 24 h intervals). Another study used closed-head CCI to inflict 3 impacts on mice with an interval of 24 h (Chen et al., 2017). Histological assessment of GFAP showed an elevated expression, which persisted 3 months after injury (Luo et al., 2014). Similar observations were also reported in rats (Brooks et al., 2017; Eyolfson et al., 2020). Therefore, it is likely that the intensity and persistence of a microglial and astrocytic response reflects at least to some extent the rmTBI protocol used (and there are numerous variations for induction of rmTBI in the literature), and also the developmental stage of the animal species and strain used. Overall, our data in the two models indicate a stronger and more persistent inflammatory response in the juvenile CD1 mouse after CCI, when compared to rmTBI.

For cellular senescence, the analysis of rmTBI tissue using

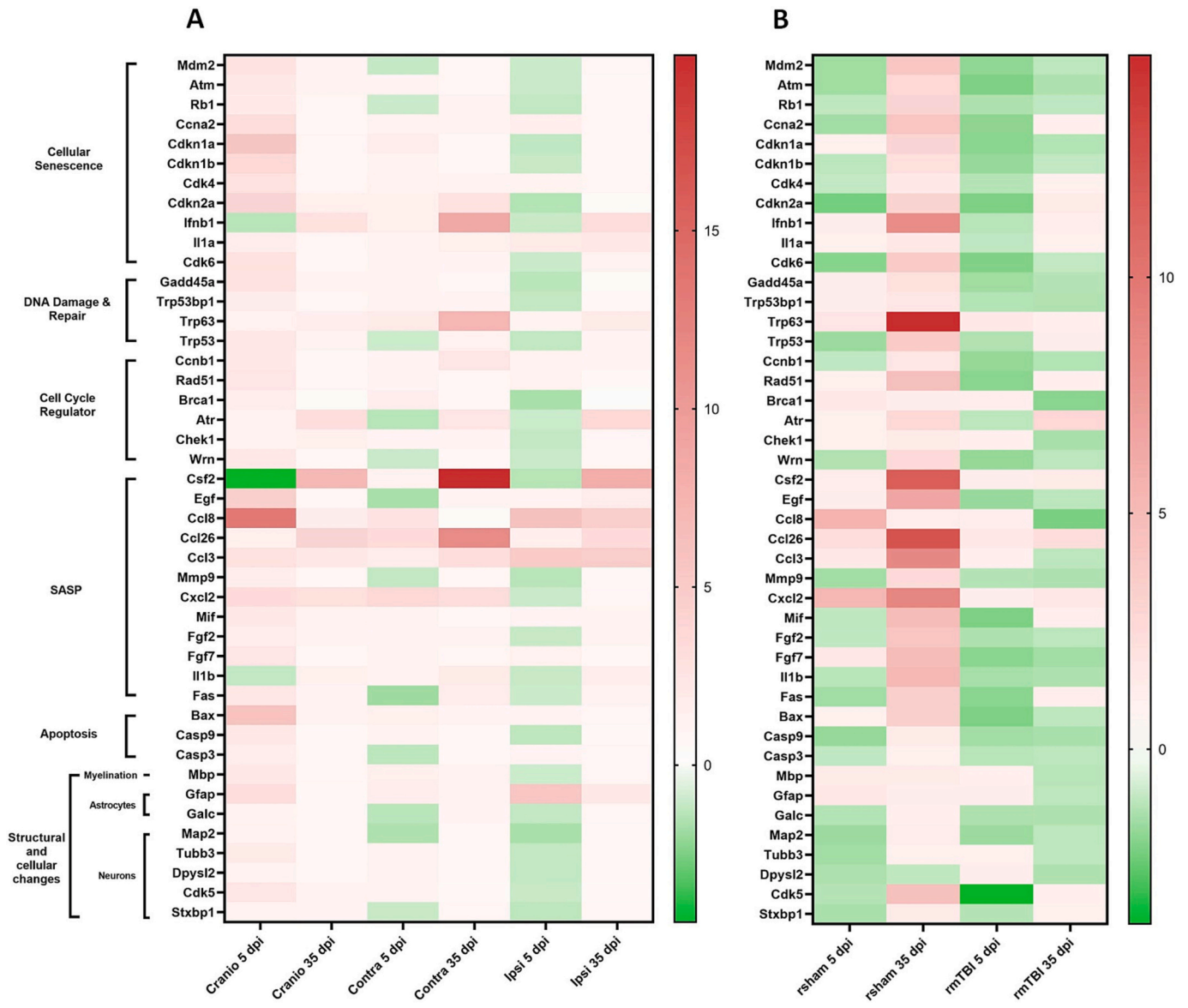

Fig. 10. Fold regulation of different genes expressed between the experimental groups and naïve mice at 5 and 35 dpi. (A) The CCI experiment (B) The rmTBI experiment. Data were analysed using the GeneGlobe analysis tool. For CCI - At 5 dpi: 4 animals for naive, 4 animals for Cranio and 5 animals for CCI. At 35 dpi: 4 animals for naive, 4 animals for Cranio and 3 animals for CCI. For rmTBI - At 5 dpi: 4 animals for naive, 4 animals for rSham and 4 animals for rmTBI. At 35 dpi: 4 animals for naive, 4 animals for rSham and 6 animals for rmTBI.

immunofluorescence showed the absence of DNA damage-induced-cellular senescence, and this was supported by the analysis of gene expression. However, results imply the possible activation of cellular senescence through SAHF pathways (Kumari and Jat, 2021) or the non-canonical activation of the telomerase reverse transcriptase (TERT) gene (Thompson and Wong, 2020). This is evident by the increased expression of p16INK4a at the protein level, and the DNA damage signalling through epigenetic changes. In contrast, CCI injury showed a clear DNA damage response (DDR) activation at the protein level in the acute phase; p16INK4a was also increased, indicating involvement of SAHF. These observations indicate the initiation of a cellular senescence response after injury. In the later phase, protein levels of the different markers were not significantly increased, however, there was a tendency to an increased expression of a major DDR marker (γH2AX/53BP1 double foci) and p16INK4a, hinting at persistent activation of different senescence pathways. This persistence was confirmed with gene expression analysis. Interestingly, p16INK4a has been linked to a maintenance role for stem cells in the dentate gyrus, protecting their self-renewal during aging (Micheli et al., 2019). The analysis of the ipsilateral hemisphere showed cellular senescence activation through a DDR; this was in contrast with the activation of DNA damage signalling through epigenetic changes in the contralateral hemisphere, suggesting the activation of SAHF or non-canonical activation of telomerase reverse transcriptase. Thus, unilateral CCI in the immature brain activated two different senescence pathways, each pathway being associated with a different hemisphere.

To our knowledge, no studies in the literature have reported similar findings regarding cellular senescence, although a few have documented a unique molecular response from the contralateral hemisphere following unilateral brain injury. In a study by White et al. (2013), rat brain tissues from both ipsilateral and contralateral hemispheres were analysed at 1 dpi following CCI. The analysis of genes related to inflammation demonstrated a bilateral activation of the inflammatory response, with 75% of all tested genes exhibiting a similar response between the two hemispheres, showing either an increase or decrease in expression. However, the remaining 25% of genes displayed a

Table 2
Fold regulation of different genes expressed between CCI experimental groups and naïve mice at 5 and 35 dpi; highlighted cells represent $p < 0.05$. Data were analysed using the GeneGlobe analysis tool. At 5 dpi: 4 animals for naive, 4 animals for Cranio and 5 animals for CCI. At 35 dpi: 4 animals for naive, 4 animals for Cranio and 3 animals for CCI.

Symbol	Function	Cranio 5dpi	Cranio 35dpi	Contra 5 dpi	Contra 35 dpi	Ipsi 5dpi	Ipsi 35 dpi
Cdkn1a	p21, cell cycle regulator	5.59	-1.1	1.6	-1.52	-1.21	**-1.34**
Ifnb1	Cytokine, DNA damage and repair mechanisms	-1.37	2.84	1.44	**8.61**	-1.09	3.19
Il1a	Cytokine, immune system response, inflammation	1.57	-1.07	1.13	1.43	**1.92**	**2.15**
Gadd45a	Growth arrest, DNA damage response	2.64	1.09	1.16	-1.15	-1.33	**-2.5**
Trp63	Transcription factor, cellular response to stress	1.33	1.58	1.88	**7.22**	1.08	1.86
Ccnb1	G2/M transition phase of the cell cycle	**2.09**	-1.54	1.06	**2.52**	1.21	1.03
Brca1	Cell cycle regulator, DNA repair mechanisms, apoptosis	1.8	-2.22	1.62	-1.35	**-1.67**	-3.11
Wrn	Helicase, DNA repair, replication, transcription, telomere maintenance	2.01	-1.31	-1.07	**-1.39**	-1.06	-1.16
Csf2	Cytokine, production of granulocytes and monocytes, immune response	-4.41	**6.98**	1.18	**19.92**	-1.41	8.12
Ccl8	SASP component, cytokine, leukocyte recruitment, immune response	13.23	1.66	2.53	-2.16	5.94	**4.71**
Ccl26	SASP, T cell modulator, cytokine, chemotactic factor	1.43	**4.08**	3.39	**11.64**	1.5	3.4
Ccl3	Cytokine, leukocyte recruitment, immune response	2.85	2.01	1.75	3.06	5	**4.81**
Cxcl2	SASP component, inflammatory mediator	3.34	**2.93**	3.76	**3.3**	-1.06	-1.11
Fas	Cell death receptor, regulation of apoptosis	2.28	1.02	-1.86	**1.75**	-1.03	1.24
Casp9	Apoptosis activator	2.19	**-1.71**	1.09	**-1.66**	-1.26	**-1.71**
Casp3	Apoptosis execution phase	**1.62**	-1.16	-1.27	-1.41	1.02	-1.06
Gfap	Astrocyte activation, neuroinflammation	3.1	**-1.77**	1.61	1.22	**5.45**	**2**
Map2	Neuritogenesis	1.3	-1.25	-1.58	**-1.44**	-1.67	**-1.64**
Dpysl2	Neuronal morphology, growth, polarity	1.26	-1.27	1.22	-1.37	-1.2	**-1.7**

proinflammatory profile in the ipsilateral hemisphere, particularly with a 95% increase in expression. On the other hand, an anti-inflammatory gene profile was noted in the contralateral hemisphere, where 75% of inflammatory genes were downregulated (White et al., 2013). Another later study from the same team assessed further the difference between the ipsilateral and contralateral hemispheres in rat CCI brain at 1 dpi. They focused on genes associated with cell death and survival. The authors showed that the ipsilateral hemisphere was characterised by an increase in cell death genes, whereas in the contralateral hemisphere there was suppression of such genes, suggesting a protective compensatory mechanism (White et al., 2016).

Signals of cellular senescence, including senescence-associated β-galactosidase (SA-βgal), p16INK4a, p21 and p53, have been reported in adult brain in the earlier phase post-CCI (Arun et al., 2020; Ritzel et al., 2019; Tominaga et al., 2019). Some evidence shows the induction of senescence in response to DDR (Schwab et al., 2021; Schwab et al., 2022). In our experiments in juvenile mice, in both models, a somewhat unexpected observation was the response of p21; at 5 days there was no change in this marker, whereas a clear downregulation of p21 was detected at 35 days. This is in contrast with the observations in adult animals – for example Tominaga et al. (2019), showed an early increase (4 days) and persistent activation of p21 (still significant at 14 days) after CCI in adult C57BL/6 J mice. We suggest that this may be linked to a possible role of p21 (which maintains senescent cell viability), in regeneration and thus pro-repair processes (Arthur and Heber-Katz, 2011); this may occur in a delayed manner post-injury and may also be dependent on the animals' developmental stage.

It is important to note that sham groups in both models showed a noticeable reaction in tissue after the sham procedure, when compared to naïve animals. In the CCI experiment, the markers indicated an induction of cellular senescence in the acute phase, which persisted in the subacute phase. Our observations in juvenile animals indicate that craniotomy was not a neutral intervention and could activate a distinct cellular response. Similarly, the sham group in the rmTBI study (exposed repeatedly to isoflurane), showed no impairments in behavioural assessment, but the cellular and molecular assessment showed a clear difference when compared to the naïve group. Changes in the subacute phase included a clear induction of cellular senescence pathways connected to DDR and SAHF. Therefore, despite the relatively brief exposure to <2 min anaesthesia each time a mild injury was carried out, immature animals showed a clear response associated with repeated anaesthesia. To our knowledge, there are no studies investigating the

Table 3
Fold regulation of different genes expressed between rmTBI experimental groups and naïve mice at 5 and 35 dpi; highlighted cells represent $p < 0.05$. Data were analysed using the GeneGlobe analysis tool. At 5 dpi: 4 animals for naive, 4 animals for rSham and 4 animals for rmTBI. At 35 dpi: 4 animals for naive, 4 animals for rSham and 6 animals for rmTBI.

Symbol	Function	rSham 5dpi	rSham 35 dpi	rmTBI 5 dpi	rmTBI 35 dpi
Atm	DNA damage and repair mechanism, cellular senescence, apoptosis	-1.55	**2.82**	-2.06	-1.33
Rb1	Cell cycle regulator	-1.06	**2.98**	-1.35	-1.04
Ccna2	Cell cycle regulator, senescence initiator	-1.49	**4.2**	-1.85	1.11
Cdkn1b	p27, negative cell cycle regulator	-1.1	**2.16**	-1.69	-1
Ifnb1	Cytokine, DNA damage and repair mechanisms	1.25	**8.38**	-1.14	1.19
Cdk6	cell cycle regulator, senescence pathways	-1.94	**3.71**	-2.01	-1.01
Trp53bp1	Promote non-homologous end joining (NHEJ) repair pathway	1.22	**1.78**	-1.23	-1.28
Trp63	DNA damage and repair mechanisms	1.85	**14.7**	1.54	1.08
Rad51	homologous recombination repair mechanism	1.06	**4.73**	-1.89	1.09
Wrn	DNA repair mechanisms	-1.28	**2.51**	-1.72	-1.1
Csf2	Cytokine	1.34	**11.7**	1.23	1.43
Egf	Growth factor	1.27	**6.47**	-1.67	-1.07
Ccl8	SASP component, mediates neuroinflammation	**5.52**	1.3	1.18	-2.12
Ccl26	SASP and a T cells mediator	2.32	**12.36**	1.55	2.36
Ccl3	Chemokine	1.52	**8.64**	1.08	-1.08
Mmp9	Breakdown of extracellular matrix	-1.49	**2.57**	-1.2	-1.31
Mif	SASP components, inflammation regulator	-1.05	**4.86**	-2.09	1.21
Fgf2	Growth factor	-1.02	**4.17**	-1.32	-1.07
Fas	Cell death receptor, apoptosis	-1.52	**3.5**	-1.86	1.16
Casp3	Apoptosis activator	-1.02	1.02	-1.15	-1.07
Cdk5	Neuronal projections of axons and dendrites	-1.21	**4.6**	-3.7	1.09

effect of isoflurane (or other halogenated anaesthetics) on cellular senescence, whether in the brain or other organs. However, one study reported increased levels of γH2AX and p53 after exposing a human cell line (H4 human neuroglioma cells) to 2% isoflurane for 3 or 6 h. Another study involved hospital professionals who were regularly exposed to isoflurane; younger individuals who were exposed to isoflurane for <5 years showed a higher level of DNA damage in leukocytes than older individuals who were exposed for the same period (Figueiredo et al., 2022). We have not found reports which used conditions strictly comparable to ours, so that we can comment and compare specifically with observations made with anaesthesia protocols used in other groups. Anaesthetics have a complex pharmacodynamics (Franks, 2006), and there are recent new insights into the multiple targets of isoflurane (Yuan et al., 2023), and clear evidence that this inhalation anaesthetic can modulate complex signalling pathways associated with cell death and inflammation (Hu et al., 2018). Therefore, the various molecular targets involved may be able to trigger senescence signals.

Finally, our studies used male animals, and clinical and experimental studies indicate differences in responses between males and females after brain injury (Berry et al., 2009; Farace and Alves, 2000; Groswasser et al., 1998; Munivenkatappa et al., 2016; Russell et al., 2018; Schwab et al., 2022; Tucker et al., 2017). Therefore, in future it will be interesting to investigate whether in a manner reported in adult animals, juvenile females have a lower senescence response in spite of higher DNA damage (Schwab et al., 2022). Furthermore, further analysis could identify the cellular types expressing the various senescence markers across time.

Regarding the timeline of various processes triggered by injury: we focused on two time points, but there is a clear indication in the literature that some changes in tissue can be very delayed and may occur months after injury (Mouzon et al., 2017). Pathology studies in repeatedly concussed professional athletes show DNA damage and senescence signals response and a deficient DNA repair, detected years after the initial concussive events (Schwab et al., 2019). It cannot be ruled out that after injury in juveniles, there may be delayed waves of senescence signals, and/or neurological outcome changes which occur much later after injury, and this remains to be investigated, by investigating later time points, and also more extensive behavioural responses.

5. Conclusion

Our results clearly indicate the activation of cellular senescence signals after injury, in parallel with neuroinflammation, in the juvenile brain. The activation of a response, both for cellular senescence and neuroinflammation, is injury mode/pattern and severity dependent. Some changes occur early and may be linked to the early

neuroinflammation and oxidative stress that occurs in tissue, whereas some delayed changes may reflect the initiation of pro-repair processes. How these are linked to the risk of subsequent risk of neurodegeneration is an area which needs to be further explored.

Funding

This research did not receive any specific grant from funding agencies in the public, commercial, or not-for-profit sectors.

CRediT authorship contribution statement

Zahra F. Al-Khateeb: Formal analysis, Investigation, Methodology, Resources, Software, Validation, Visualization, Writing – original draft. **Hasna Boumenar:** Investigation. **Joycee Adebimpe:** Investigation. **Shenel Shekerzade:** Investigation. **Siân M. Henson:** Methodology, Supervision, Writing – review & editing. **Jordi L. Tremoleda:** Conceptualization, Methodology, Resources, Supervision, Validation, Writing – review & editing. **Adina T. Michael-Titus:** Conceptualization, Methodology, Project administration, Supervision, Writing – review & editing.

Declaration of competing interest

None, the authors declare no competing interests.

Data availability

Data will be made available on request.

Acknowledgments

We would like to thank Professor Cleo Bishop for her suggestions during the planning and development of this research and Dr. Luke Gammon for his assistance in writing and revising scanning and quantification protocols.

Appendix A. Supplementary data

Supplementary data to this article can be found online at https://doi.org/10.1016/j.expneurol.2024.114714.

References

Araki, T., Yokota, H., Morita, A., 2017 Feb 15. Pediatric traumatic brain injury: characteristic features, diagnosis, and management. Neurol. Med. Chir. (Tokyo) 57 (2), 82–93. https://doi.org/10.2176/nmc.ra.2016-0191. Epub 2017 Jan 20. PMID: 28111406; PMCID: PMC5341344.

Arthur, L.M., Heber-Katz, E., 2011 Jun 29. The role of p21 in regulating mammalian regeneration. Stem Cell Res Ther 2 (3), 30. https://doi.org/10.1186/scrt71. PMID: 21722344; PMCID: PMC3152998.

Arun, P., Rossetti, F., Wilder, D.M., Sajja, S., Van Albert, S.A., Wang, Y., Gist, I.D., Long, J.B., 2020 May 21. Blast exposure leads to accelerated cellular senescence in the rat brain. Front. Neurol. (11), 438. https://doi.org/10.3389/fneur.2020.00438. PMID: 32508743; PMCID: PMC7253679.

Baker, D.J., Petersen, R.C., 2018 Apr 2. Cellular senescence in brain aging and neurodegenerative diseases: evidence and perspectives. J. Clin. Invest. 128 (4), 1208–1216. https://doi.org/10.1172/JCI95145. Epub 2018 Feb 19. PMID: 29457783; PMCID: PMC5873891.

Beni-Adani, L., Gozes, I., Cohen, Y., Assaf, Y., Steingart, R.A., Brenneman, D.E., Eizenberg, O., Trembolver, V., Shohami, E., 2001 Jan. A peptide derived from activity-dependent neuroprotective protein (ADNP) ameliorates injury response in closed head injury in mice. J. Pharmacol. Exp. Ther. 296 (1), 57–63. PMID: 11123362.

Berry, C., Ley, E.J., Tillou, A., Cryer, G., Margulies, D.R., Salim, A., 2009 Nov. The effect of gender on patients with moderate to severe head injuries. J. Trauma 67 (5), 950–953. https://doi.org/10.1097/TA.0b013e3181ba3354. PMID: 19901653.

Bittigau, P., Pohl, D., Sifringer, M., Shimizu, H., Ikeda, M., Ishimaru, M., Stadthaus, D., Fuhr, S., Dikranian, K., Olney, J.W., Ikonomidou, C., 1998. Modeling pediatric head trauma: mechanisms of degeneration and potential strategies for neuroprotection. Restor. Neurol. Neurosci. 13 (1–2), 11–23 (PMID: 12671284).

Brooks, D.M., Patel, S.A., Wohlgehagen, E.D., Semmens, E.O., Pearce, A., Sorich, E.A., Rau, T.F., 2017 Nov. Multiple mild traumatic brain injury in the rat produces persistent pathological alterations in the brain. Exp. Neurol. 297, 62–72. https://doi.org/10.1016/j.expneurol.2017.07.015. Epub 2017 Jul 27. PMID: 28756201.

Byrnes, K.R., Faden, A.I., 2007 Oct. Role of cell cycle proteins in CNS injury. Neurochem. Res. 32 (10), 1799–1807. https://doi.org/10.1007/s11064-007-9312-2. Epub 2007 Apr 3. PMID: 17404835.

Cappa, K.A., Conger, J.C., Conger, A.J., 2011 Sep. Injury severity and outcome: a meta-analysis of prospective studies on TBI outcome. Health Psychol. 30 (5), 542–560. https://doi.org/10.1037/a0025220. PMID: 21875208.

Carreno, G., Guiho, R., Martinez-Barbera, J.P., 2021 Apr. Cell senescence in neuropathology: A focus on neurodegeneration and tumours. Neuropathol. Appl. Neurobiol. 47 (3), 359–378. https://doi.org/10.1111/nan.12689. Epub 2021 Feb 1. PMID: 33378554; PMCID: PMC8603933.

Chen, H., Desai, A., Kim, H.Y., 2017 Jul 15. Repetitive closed-head impact model of engineered rotational acceleration induces long-term cognitive impairments with persistent astrogliosis and microgliosis in mice. J. Neurotrauma 34 (14), 2291–2302. https://doi.org/10.1089/neu.2016.4870. Epub 2017 Apr 26. PMID: 28288551; PMCID: PMC5510798.

Chen, C., Peng, J., Sribnick, E.A., Zhu, M., Xiang, H., 2018 Jun 5. Trend of age-adjusted rates of pediatric traumatic brain injury in U.S. Emergency Departments from 2006 to 2013. Int. J. Environ. Res. Public Health 15 (6), 1171. https://doi.org/10.3390/ijerph15061171. PMID: 29874782; PMCID: PMC6024977.

Cole, W.R., Gerring, J.P., Gray, R.M., Vasa, R.A., Salorio, C.F., Grados, M., Christensen, J. R., Slomine, B.S., 2008 Nov. Prevalence of aggressive behaviour after severe paediatric traumatic brain injury. Brain Inj. 22 (12), 932–939. https://doi.org/10.1080/02699050802454808. PMID: 19005885; PMCID: PMC2782953.

Dennis, M., Spiegler, B.J., Simic, N., Sinopoli, K.J., Wilkinson, A., Yeates, K.O., Taylor, H. G., Bigler, E.D., Fletcher, J.M., 2014 Dec. Functional plasticity in childhood brain disorders: when, what, how, and whom to assess. Neuropsychol. Rev. 24 (4), 389–408. https://doi.org/10.1007/s11065-014-9261-x. Epub 2014 May 13. PMID: 24821533; PMCID: PMC4231018.

Donat, C.K., Scott, G., Gentleman, S.M., Sastre, M., 2017 Jun 28. Microglial activation in traumatic brain injury. Front. Aging Neurosci. (9), 208. https://doi.org/10.3389/fnagi.2017.00208. PMID: 28701948; PMCID: PMC5487478.

Dutta, S., Sengupta, P., 2016 May 1. Men and mice: relating their ages. Life Sci. (152), 244–248. https://doi.org/10.1016/j.lfs.2015.10.025. Epub 2015 Oct 24. PMID: 26596563.

Ertürk, A., Mentz, S., Stout, E.E., Hedehus, M., Dominguez, S.L., Neumaier, L., Krammer, F., Llovera, G., Srinivasan, K., Hansen, D.V., Liesz, A., Scearce-Levie, K.A., Sheng, M., 2016 Sep 21. Interfering with the chronic immune response rescues chronic degeneration after traumatic brain injury. J. Neurosci. 36 (38), 9962–9975. https://doi.org/10.1523/JNEUROSCI.1898-15.2016. PMID: 27656033; PMCID: PMC6705567.

Ewing-Cobbs, L., Prasad, M.R., Kramer, L., Cox Jr., C.S., Baumgartner, J., Fletcher, S., Mendez, D., Barnes, M., Zhang, X., Swank, P., 2006 Oct. Late intellectual and academic outcomes following traumatic brain injury sustained during early childhood. J. Neurosurg. 105 (4 Suppl), 287–296. https://doi.org/10.3171/ped.2006.105.4.287. PMID: 17328279; PMCID: PMC2615233.

Eyolfson, E., Yamakawa, G.R., Griep, Y., Collins, R., Carr, T., Wang, M., Lohman, A.W., Mychasiuk, R., 2020 Feb 20. Examining the progressive behavior and neuropathological outcomes associated with chronic repetitive mild traumatic brain injury in rats. Cereb Cortex Commun 1 (1). https://doi.org/10.1093/texcom/tgaa002 tgaa002. PMID: 34296084; PMCID: PMC8152839.

Farace, E., Alves, W.M., 2000. Do women fare worse? A metaanalysis of gender differences in outcome after traumatic brain injury. Neurosurg. Focus. 8 (1), e6 https://doi.org/10.3171/foc.2000.8.1.152 (PMID: 16924776).

Fehily, B., Fitzgerald, M., 2017 Jul. Repeated mild traumatic brain injury: potential mechanisms of damage. Cell Transplant. 26 (7), 1131–1155. https://doi.org/10.1177/0963689717714092. PMID: 28933213; PMCID: PMC5657727.

Fenn, A.M., Gensel, J.C., Huang, Y., Popovich, P.G., Lifshitz, J., Godbout, J.P., 2014 Oct 1. Immune activation promotes depression 1 month after diffuse brain injury: a role for primed microglia. Biol. Psychiatry 76 (7), 575–584. https://doi.org/10.1016/j.biopsych.2013.10.014. Epub 2013 Oct 25. PMID: 24289885; PMCID: PMC4000292.

Figueiredo, D.B.S., Aun, A.G., Souza, K.M., Nishimoto, I.H., Silva, M.A.P., de Carvalho, L. R., Braz, L.G., Braz, M.G., 2022 Oct. High anesthetic (isoflurane) indoor pollution is associated with genetic instability, cytotoxicity, and proliferative alterations in professionals working in a veterinary hospital. Environ. Sci. Pollut. Res. Int. 29 (47), 71774–71784. https://doi.org/10.1007/s11356-022-20444-2. Epub 2022 May 23. PMID: 35606583.

Folch, J., Junyent, F., Verdaguer, E., Auladell, C., Pizarro, J.G., Beas-Zarate, C., Pallàs, M., Camins, A., 2012 Oct. Role of cell cycle re-entry in neurons: a common apoptotic mechanism of neuronal cell death. Neurotox. Res. 22 (3), 195–207. https://doi.org/10.1007/s12640-011-9277-4. Epub 2011 Oct 1. PMID: 21965004.

Frade, J.M., Ovejero-Benito, M.C., 2015. Neuronal cell cycle: the neuron itself and its circumstances. Cell Cycle 14 (5), 712–720. https://doi.org/10.1080/15384101.2015.1004937. PMID: 25590687; PMCID: PMC4418291.

Franks, N.P., 2006 Jan. Molecular targets underlying general anaesthesia. Br. J. Pharmacol. 147 Suppl 1 (Suppl. 1), S72–S81. https://doi.org/10.1038/sj.bjp.0706441. PMID: 16402123; PMCID: PMC1760740.

Gottlieb, A., Toledano-Furman, N., Prabhakara, K.S., Kumar, A., Caplan, H.W., Bedi, S., Cox Jr., C.S., Olson, S.D., 2022 Apr 15. Time dependent analysis of rat microglial surface markers in traumatic brain injury reveals dynamics of distinct cell subpopulations. Sci. Rep. 12 (1), 6289. https://doi.org/10.1038/s41598-022-10419-1. PMID: 35428862; PMCID: PMC9012748.

Greene, L.A., Biswas, S.C., Liu, D.X., 2004 Jan. Cell cycle molecules and vertebrate neuron death: E2F at the hub. Cell Death Differ. 11 (1), 49–60. https://doi.org/10.1038/sj.cdd.4401341. PMID: 14647236.

Groswasser, Z., Cohen, M., Keren, O., 1998 Sep. Female TBI patients recover better than males. Brain Inj. 12 (9), 805–808. https://doi.org/10.1080/026990598122197. PMID: 9755371.

Halstead, M.E., Walter, K.D., Moffatt, K., 2018. Sport-related concussion in children and adolescents. Pediatrics 142 (6), e20183074.

Hirad, A.A., Bazarian, J.J., Merchant-Borna, K., Garcea, F.E., Heilbronner, S., Paul, D., Hintz, E.B., van Wijngaarden, E., Schifitto, G., Wright, D.W., Espinoza, T.R., Mahon, B.Z., 2019 Aug 7. A common neural signature of brain injury in concussion and subconcussion. Sci. Adv. 5 (8), eaau3460. https://doi.org/10.1126/sciadv.aau3460. PMID: 31457074; PMCID: PMC6685720.

Hoogenboom, W.S., Branch, C.A., Lipton, M.L., 2019 Jun. Animal models of closed-skull, repetitive mild traumatic brain injury. Pharmacol. Ther. 198, 109–122. https://doi.org/10.1016/j.pharmthera.2019.02.016. Epub 2019 Feb 26. PMID: 30822463; PMCID: PMC6536340.

Hu, J., Hu, J., Jiao, H., Li, Q., 2018 Jul. Anesthetic effects of isoflurane and the molecular mechanism underlying isoflurane-inhibited aggressiveness of hepatic carcinoma. Mol Med Rep 18 (1), 184–192. https://doi.org/10.3892/mmr.2018.8945. Epub 2018 May 2. PMID: 29749446; PMCID: PMC6059668.

Janatpour, Z.C., Korotcov, A., Bosomtwi, A., Dardzinski, B.J., Symes, A.J., 2019 Nov 15. Subcutaneous administration of angiotensin-(1-7) improves recovery after traumatic brain injury in mice. J. Neurotrauma 36 (22), 3115–3131. https://doi.org/10.1089/neu.2019.6376. Epub 2019 Jun 17. PMID: 31037999.

Kabadi, S.V., Stoica, B.A., Loane, D.J., Byrnes, K.R., Hanscom, M., Cabatbat, R.M., Tan, M.T., Faden, A.I., 2012 Mar 20. Cyclin D1 gene ablation confers neuroprotection in traumatic brain injury. J. Neurotrauma 29 (5), 813–827. https://doi.org/10.1089/neu.2011.1980. Epub 2012 Jan 13. PMID: 21895533; PMCID: PMC3303105.

Katano, H., Masago, A., Taki, H., Nakatsuka, M., Fuse, T., Yamada, K., 2000 Jul 14. p53-independent transient p21(WAF1/CIP1) mRNA induction in the rat brain following experimental traumatic injury. Neuroreport. 11 (10), 2073–2078. https://doi.org/10.1097/00001756-200007140-00003. PMID: 10923646.

Kennedy, L., Nuno, M., Gurkoff, G.G., Nosova, K., Zwienenberg, M., 2022 Aug 3. Moderate and severe TBI in children and adolescents: the effects of age, sex, and injury severity on patient outcome 6 months after injury. Front. Neurol. (13), 741717 https://doi.org/10.3389/fneur.2022.741717. PMID: 35989939; PMCID: PMC9382186.

Kuhtz-Buschbeck, J.P., Hoppe, B., Gölge, M., Dreesmann, M., Damm-Stünitz, U., Ritz, A., 2003 Dec. Sensorimotor recovery in children after traumatic brain injury: analyses of gait, gross motor, and fine motor skills. Dev. Med. Child Neurol. 45 (12), 821–828. https://doi.org/10.1017/s001216220300152x. PMID: 14667074.

Kumari, R., Jat, P., 2021 Mar 29. Mechanisms of cellular senescence: cell cycle arrest and senescence associated secretory phenotype. Front. Cell Dev. Biol. (9), 645593 https://doi.org/10.3389/fcell.2021.645593. PMID: 33855023; PMCID: PMC8039141.

Lavender, A.P., Rawlings, S., Warnock, A., McGonigle, T., Hiles-Murison, B., Nesbit, M., Lam, V., Hackett, M.J., Fitzgerald, M., Takechi, R., 2020 May 29. Repeated long-term sub-concussion impacts induce motor dysfunction in rats: a potential rodent model. Front. Neurol. 11, 491. https://doi.org/10.3389/fneur.2020.00491. PMID: 32547485; PMCID: PMC7274030.

Luo, J., Nguyen, A., Villeda, S., Zhang, H., Ding, Z., Lindsey, D., Bieri, G., Castellano, J. M., Beaupre, G.S., Wyss-Coray, T., 2022 Jun 29. Long-term cognitive impairments and pathological alterations in a mouse model of repetitive mild traumatic brain injury. Front Neurol. 2014 Feb 4 ;5:12. Doi: 10.3389/fneur.2014.00012. Erratum in: Front. Neurol. 13, 730576. PMID: 24550885; PMCID: PMC3912443.

McAllister, T., McCrea, M., 2017 Mar. Long-term cognitive and neuropsychiatric consequences of repetitive concussion and head-impact exposure. J. Athl. Train. 52 (3), 309–317. https://doi.org/10.4085/1062-6050-52.1.14. PMID: 28387556; PMCID: PMC5384827.

Mckee, A.C., Daneshvar, D.H., 2015. The neuropathology of traumatic brain injury. Handb. Clin. Neurol. 127, 45–66. https://doi.org/10.1016/B978-0-444-52892-6.00004-0. PMID: 25702209; PMCID: PMC4694720.

Micheli, L., D'Andrea, G., Ceccarelli, M., Ferri, A., Scardigli, R., Tirone, F., 2019 Feb 7. p16Ink4a prevents the activation of aged quiescent dentate gyrus stem cells by physical exercise. Front. Cell. Neurosci. 13, 10. https://doi.org/10.3389/fncel.2019.00010. PMID: 30792628; PMCID: PMC6374340.

Mira, R.G., Lira, M., Cerpa, W., 2021 Oct 22. Traumatic brain injury: mechanisms of glial response. Front. Physiol. (12), 740939 https://doi.org/10.3389/fphys.2021.740939. PMID: 34744783; PMCID: PMC8569708.

Montenigro, P.H., Bernick, C., Cantu, R.C., 2015 May. Clinical features of repetitive traumatic brain injury and chronic traumatic encephalopathy. Brain Pathol. 25 (3), 304–317. https://doi.org/10.1111/bpa.12250. PMID: 25904046; PMCID: PMC8029369.

Mouzon, B.C., Bachmeier, C., Ojo, J.O., Acker, C.M., Ferguson, S., Paris, D., Ait-Ghezala, G., Crynen, G., Davies, P., Mullan, M., Stewart, W., Crawford, F., 2017 Dec 14. Lifelong behavioral and neuropathological consequences of repetitive mild traumatic brain injury. Ann. Clin. Transl. Neurol. 5 (1), 64–80. https://doi.org/10.1002/acn3.510. PMID: 29376093; PMCID: PMC5771321.

Munivenkatappa, A., Agrawal, A., Shukla, D.P., Kumaraswamy, D., Devi, B.I., 2016 Apr-Jun. Traumatic brain injury: Does gender influence outcomes? Int J Crit Illn Inj Sci 6 (2), 70–73. https://doi.org/10.4103/2229-5151.183024. PMID: 27308254; PMCID: PMC4901830.

Ritzel, R.M., Doran, S.J., Glaser, E.P., Meadows, V.E., Faden, A.I., Stoica, B.A., Loane, D. J., 2019 May. Old age increases microglial senescence, exacerbates secondary neuroinflammation, and worsens neurological outcomes after acute traumatic brain injury in mice. Neurobiol. Aging 77, 194–206. https://doi.org/10.1016/j.neurobiolaging.2019.02.010. Epub 2019 Feb 20. PMID: 30904769; PMCID: PMC6486858.

Rosema, S., Crowe, L., Anderson, V., 2012 May 1. Social function in children and adolescents after traumatic brain injury: a systematic review 1989-2011. J. Neurotrauma 29 (7), 1277–1291. https://doi.org/10.1089/neu.2011.2144. Epub 2012 Apr 2. PMID: 22260408.

Rosenbaum, P.E., Locandro, C., Chrisman, S.P.D., Choe, M.C., Richards, R., Pacchia, C., Cook, L.J., Rivara, F.P., Gioia, G.A., Giza, C.C., 2020 Nov 2. Characteristics of pediatric mild traumatic brain injury and recovery in a concussion clinic population. JAMA Netw. Open 3 (11), e2021463. https://doi.org/10.1001/jamanetworkopen.2020.21463. PMID: 33196804; PMCID: PMC7670312.

Russell, A.L., Richardson, M.R., Bauman, B.M., Hernandez, I.M., Saperstein, S., Handa, R. J., Wu, T.J., 2018 Jun 1. Differential responses of the HPA axis to mild blast traumatic brain injury in male and female mice. Endocrinology. 159 (6), 2363–2375. https://doi.org/10.1210/en.2018-00203. PMID: 29701827.

Schober, M.E., Block, B., Beachy, J.C., Statler, K.D., Giza, C.C., Lane, R.H., 2010 Nov. Early and sustained increase in the expression of hippocampal IGF-1, but not EPO, in a developmental rodent model of traumatic brain injury. J. Neurotrauma 27 (11), 2011–2020. https://doi.org/10.1089/neu.2009.1226. PMID: 20822461; PMCID: PMC6468946.

Schwab, N., Grenier, K., Hazrati, L.N., 2019 Nov 14. DNA repair deficiency and senescence in concussed professional athletes involved in contact sports. Acta Neuropathol. Commun. 7 (1), 182. https://doi.org/10.1186/s40478-019-0822-3. PMID: 31727161; PMCID: PMC6857343.

Schwab, N., Ju, Y., Hazrati, L.N., 2021 May 8. Early onset senescence and cognitive impairment in a murine model of repeated mTBI. Acta Neuropathol. Commun. 9 (1), 82. https://doi.org/10.1186/s40478-021-01190-x. PMID: 33964983; PMCID: PMC8106230.

Schwab, N., Taskina, D., Leung, E., Innes, B.T., Bader, G.D., Hazrati, L.N., 2022 Nov 3. Neurons and glial cells acquire a senescent signature after repeated mild traumatic brain injury in a sex-dependent manner. Front. Neurosci. (16), 1027116. https://doi.org/10.3389/fnins.2022.1027116. PMID: 36408415; PMCID: PMC9669743.

Sharpless, N.E., Sherr, C.J., 2015 Aug. Forging a signature of in vivo senescence. Nat Rev Cancer. 2015 Jul;15(7):397–408. Doi: 10.1038/nrc3960. Erratum in: Nat. Rev. Cancer 15 (8), 509. PMID: 26105537.

Sikora, E., Bielak-Zmijewska, A., Dudkowska, M., Krzystyniak, A., Mosieniak, G., Wesierska, M., Wlodarczyk, J., 2021 Feb 25. Cellular senescence in brain aging. Front. Aging Neurosci. (13), 646924 https://doi.org/10.3389/fnagi.2021.646924. PMID: 33732142; PMCID: PMC7959760.

Smith, A.C., Holden, R.C., Rasmussen, S.M., Hoane, M.R., Hylin, M.J., 2019 May 17. Effects of nicotinamide on spatial memory and inflammation after juvenile traumatic brain injury. Behav. Brain Res. 364, 123–132. https://doi.org/10.1016/j.bbr.2019.02.024. Epub 2019 Feb 13. PMID: 30771366.

Spilsbury, A., Miwa, S., Attems, J., Saretzki, G., 2015 Jan 28. The role of telomerase protein TERT in Alzheimer's disease and in tau-related pathology in vitro. J. Neurosci. 35 (4), 1659–1674. https://doi.org/10.1523/JNEUROSCI.2925-14.2015. PMID: 25632141; PMCID: PMC4308607.

Stoica, B.A., Byrnes, K.R., Faden, A.I., 2009 Oct. Cell cycle activation and CNS injury. Neurotox. Res. 16 (3), 221–237. https://doi.org/10.1007/s12640-009-9050-0. Epub 2009 Apr 21. PMID: 19526282.

Thau-Zuchman, O., Gomes, R.N., Dyall, S.C., Davies, M., Priestley, J.V., Groenendijk, M., De Wilde, M.C., Tremoleda, J.L., Michael-Titus, A.T., 2019 Jan 1. Brain phospholipid precursors administered post-injury reduce tissue damage and improve neurological outcome in experimental traumatic brain injury. J. Neurotrauma 36 (1), 25–42. https://doi.org/10.1089/neu.2017.5579. Epub 2018 Jul 25. PMID: 29768974; PMCID: PMC6306688.

Thau-Zuchman, O., Ingram, R., Harvey, G.G., Cooke, T., Palmas, F., Pallier, P.N., Brook, J., Priestley, J.V., Dalli, J., Tremoleda, J.L., Michael-Titus, A.T., 2020 Jan 1. A single injection of docosahexaenoic acid induces a pro-resolving lipid mediator profile in the injured tissue and a long-lasting reduction in neurological deficit after traumatic brain injury in mice. J. Neurotrauma 37 (1), 66–79. https://doi.org/10.1089/neu.2019.6420. Epub 2019 Sep 6. PMID: 31256709.

Thau-Zuchman, O., Svendsen, L., Dyall, S.C., Paredes-Esquivel, U., Rhodes, M., Priestley, J.V., Feichtinger, R.G., Kofler, B., Lotstra, S., Verkuyl, J.M., Hageman, R.J., Broersen, L.M., van Wijk, N., Silva, J.P., Tremoleda, J.L., Michael-Titus, A.T., 2021 Jan 1. A new ketogenic formulation improves functional outcome and reduces tissue loss following traumatic brain injury in adult mice. Theranostics. 11 (1), 346–360. https://doi.org/10.7150/thno.48995. PMID: 33391479; PMCID: PMC7681084.

Thompson, C.A.H., Wong, J.M.Y., 2020. Non-canonical functions of telomerase reverse transcriptase: emerging roles and biological relevance. Curr. Top. Med. Chem. 20 (6), 498–507. https://doi.org/10.2174/1568026620666200131125110 (PMID: 32003692).

Tominaga, T., Shimada, R., Okada, Y., Kawamata, T., Kibayashi, K., 2019 Mar 11. Senescence-associated-β-galactosidase staining following traumatic brain injury in the mouse cerebrum. PLoS One 14 (3), e0213673. https://doi.org/10.1371/journal.pone.0213673. PMID: 30856215; PMCID: PMC6411151.

Tsenter, J., Beni-Adani, L., Assaf, Y., Alexandrovich, A.G., Trembovler, V., Shohami, E., 2008 Apr. Dynamic changes in the recovery after traumatic brain injury in mice: effect of injury severity on T2-weighted MRI abnormalities, and motor and cognitive functions. J. Neurotrauma 25 (4), 324–333. https://doi.org/10.1089/neu.2007.0452. PMID: 18373482.

Tucker, L.B., Burke, J.F., Fu, A.H., McCabe, J.T., 2017 Feb 15. Neuropsychiatric symptom modeling in male and female C57BL/6J mice after experimental traumatic

brain injury. J. Neurotrauma 34 (4), 890–905. https://doi.org/10.1089/neu.2016.4508. Epub 2016 Jun 7. PMID: 27149139; PMCID: PMC5314988.

Van Deynse, H., Van Belleghem, G., Lauwaert, D., Moens, M., Pien, K., Devos, S., Hubloue, I., Putman, K., 2019. The incremental cost of traumatic brain injury during the first year after a road traffic accident. Brain Inj. 33 (9), 1234–1244. https://doi.org/10.1080/02699052.2019.1641224. Epub 2019 Jul 12. PMID: 31298587.

Vazquez-Villaseñor, I., Garwood, C.J., Heath, P.R., Simpson, J.E., Ince, P.G., Wharton, S. B., 2020 Feb. Expression of p16 and p21 in the frontal association cortex of ALS/MND brains suggests neuronal cell cycle dysregulation and astrocyte senescence in early stages of the disease. Neuropathol. Appl. Neurobiol. 46 (2), 171–185. https://doi.org/10.1111/nan.12559. Epub 2019 Jun 17. PMID: 31077599; PMCID: PMC7217199.

White, T.E., Ford, G.D., Surles-Zeigler, M.C., Gates, A.S., Laplaca, M.C., Ford, B.D., 2013 Apr 25. Gene expression patterns following unilateral traumatic brain injury reveals a local pro-inflammatory and remote anti-inflammatory response. BMC Genomics (14), 282. https://doi.org/10.1186/1471-2164-14-282. PMID: 23617241; PMCID: PMC3669032.

White, T.E., Surles-Zeigler, M.C., Ford, G.D., Gates, A.S., Davids, B., Distel, T., LaPlaca, M.C., Ford, B.D., 2016 Feb 24. Bilateral gene interaction hierarchy analysis of the cell death gene response emphasizes the significance of cell cycle genes following unilateral traumatic brain injury. BMC Genomics (17), 130. https://doi.org/10.1186/s12864-016-2412-0. PMID: 26912237; PMCID: PMC4765060.

Yu, G., Zhang, Y., Ning, B., 2021 Dec 23. Reactive astrocytes in central nervous system injury: subgroup and potential therapy. Front. Cell. Neurosci. (15), 792764 https://doi.org/10.3389/fncel.2021.792764. PMID: 35002629; PMCID: PMC8733560.

Yuan, M., Wu, H., 2022 Feb. Astrocytes in the traumatic brain injury: the good and the bad. Exp. Neurol. 348, 113943 https://doi.org/10.1016/j.expneurol.2021.113943. Epub 2021 Dec 2. PMID: 34863998.

Yuan, H., Yang, S., Han, P., Sun, M., Zhou, C., 2023 Dec 6. Drug target genes and molecular mechanism investigation in isoflurane-induced anesthesia based on WGCNA and machine learning methods. Toxicol. Mech. Methods 1–15. https://doi.org/10.1080/15376516.2023.2286619. Epub ahead of print. PMID: 38054380.